Spoke 6: Ecological transition based on HPC and data technology

Proteggere le acque sotterranee con i supercalcolatori: modellazione e simulazione della migrazione di contaminanti nel sottosuolo

Workshop “Ricerca, Sostenibilità e Rigenerazione”
13 Febbraio 2026
COMP-R SCVSA UNIPR

DIPARTIMENTO DI ECCELLENZA
2018-2022
2023-2027

Alessandra Feo

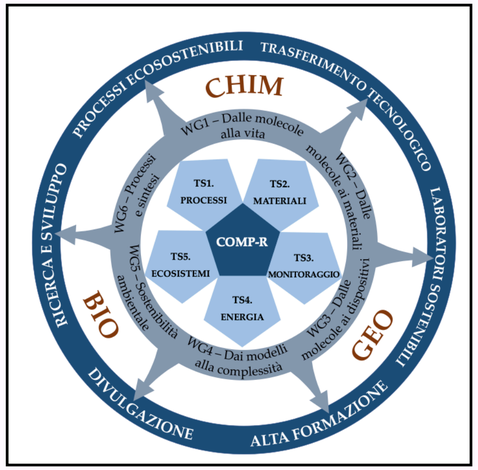

Cosa simuliamo?

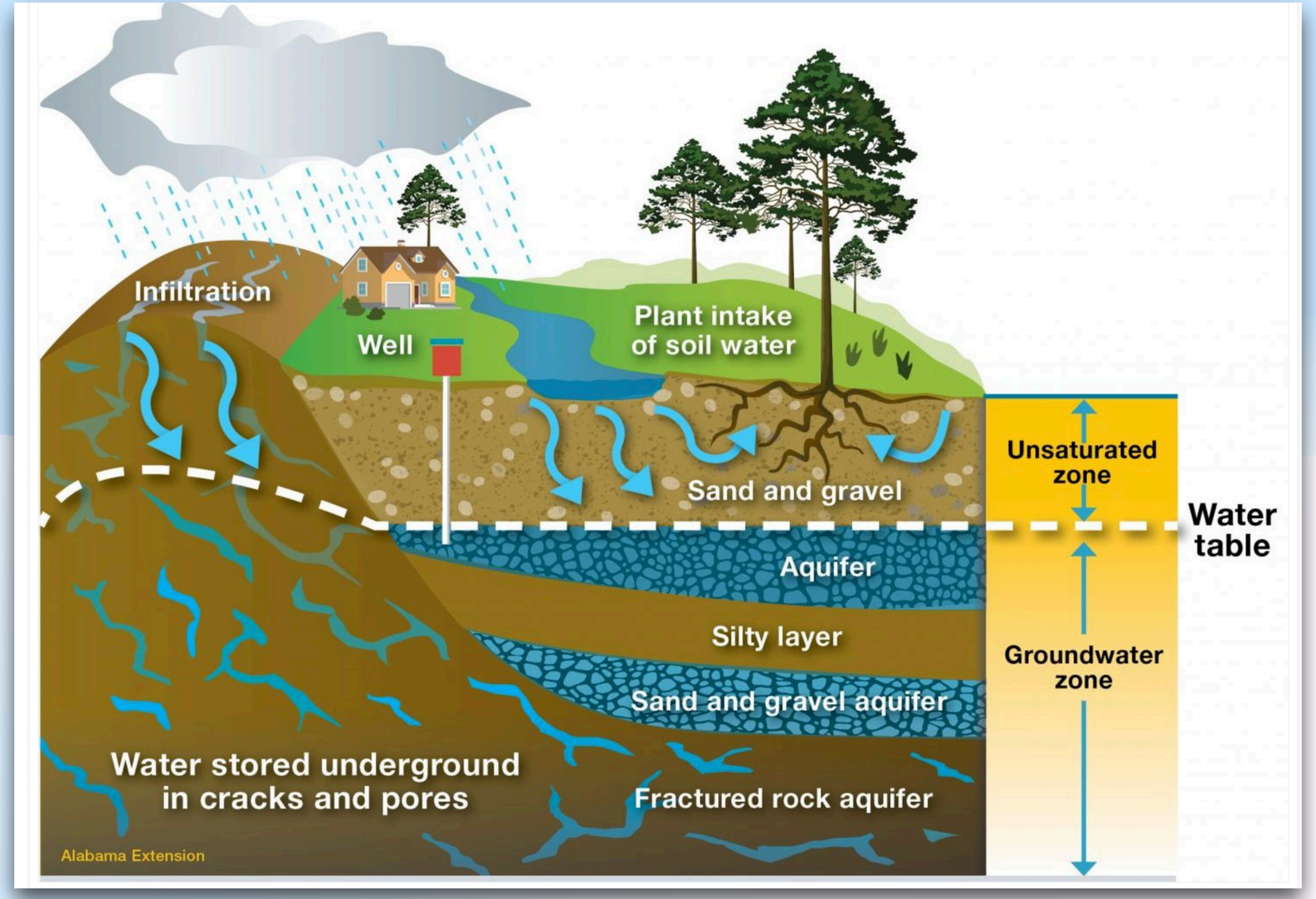

- Simulation of flow and contaminant transport. Saturation contour profiles of the three-phase fluid flow (water + contaminant + air) in variably saturated zones. High-resolution in space and time.
- The increased computational speed and capacity of present day multicore computers, the and new powerful codes that provide enhanced modeling tools are revolutionizing the science of groundwater modeling.
- In the past, details of the actual movement of water through the unsaturated zone have been of little or no interest. The situation has completely changed with the rising interest in subsurface contamination.
- In recent years, public attention has been focused on groundwater contamination by hazardous industrial wastes, on leachate from landfills and spills of oil and other toxic liquids, on agricultural activities, such as the use of fertilizers, pesticides, and herbicides, and on radioactive waste in repositories located in deep geological formations.
- Any plan of mitigation, cleanup operations, or control measures, once contamination has been detected in the subsurface, requires the prediction of pathways and fate of the contaminants, in response to certain planned remediation activities.
- Multidisciplinary research involves collaboration among experts from different academic fields who apply their respective methodologies and knowledge to a common, complex problem.

Plan of the Talk

- The problem and the solution: contaminant transport using computational fluid dynamics (CFD)
- Mathematical setup
- Applications to the migration of LNAPL and DNAPL in unsaturated/saturated zones to make predictions in space and time:
    - In oil pipelines (spilled fixed term benzene, gasoil oil, petroleum)
    - In homogeneous and heterogeneous multilayered shallow and deep aquifers
    - In sand column experiments (spilled oil)

LNAPL (Light NAPL) and DNAPL (Dense NAPL): The Problem

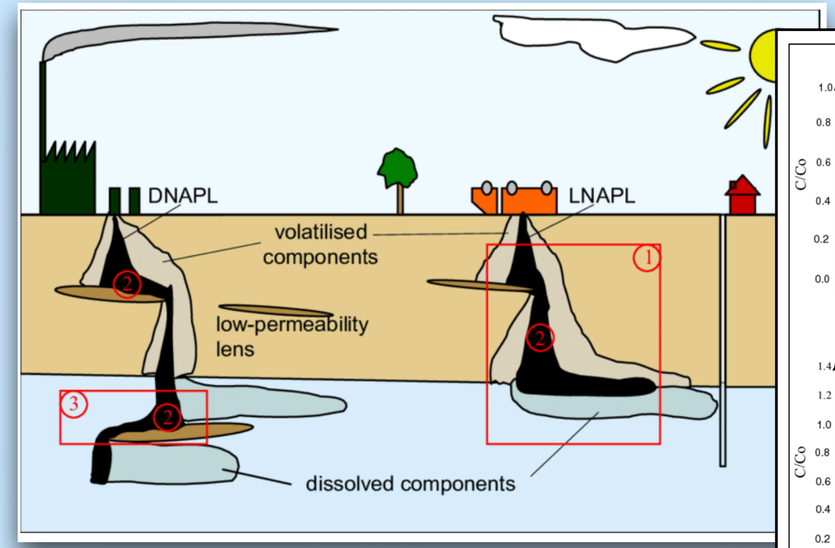

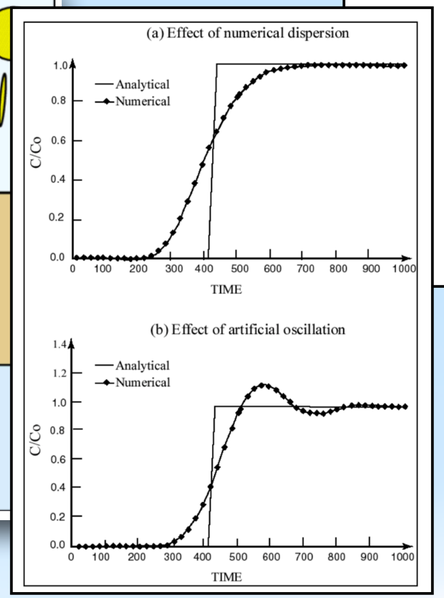

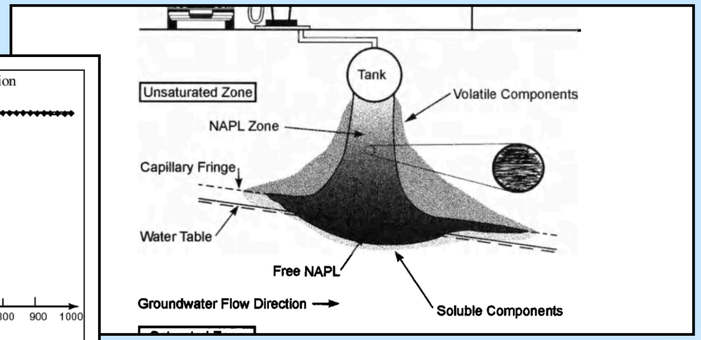

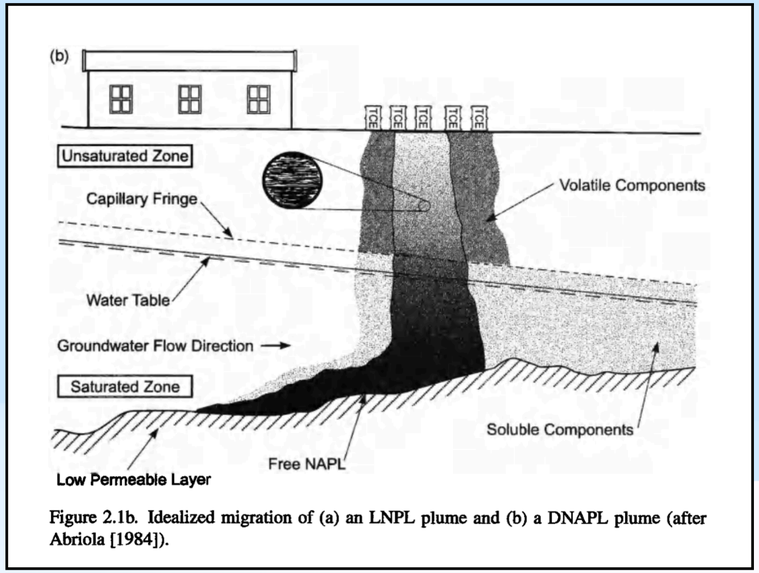

Figure 2.1b. Idealized migration of (a) an LNPL plume and (b) a DNAPL plume (after Abriola [1984]).

- After being released into the environment, the immiscible contaminant infiltrates the porous medium, from the unsaturated zone to the saturated one under the influence of gravity.
- From a numerical point of view, the resulting dynamics are very complex, since capillary pressure and permeability depend on the saturation. The resulting dynamics are highly nonlinear and create sharp discontinuities called ‘shocks front’ which, if not adequately treated, introduce significant numerical errors in the simulations.
- In the literature, this dynamics is separated into different steps (the unsaturated zone (vertical) separated from the saturated zone (horizontal), the LNAPL from the DNAPL), etc. The vertical (1D) is treated with an analytical code (Hydrocarbon spill screening model (HSSM)), and the horizontal with MT3DMS, etc.
- **The solution**: Using a high-resolution shock-capturing conservative method to resolve the nonlinear governing partial differential equations of a three-phase fluid flow allows to treat the system through both zones and accurately tracking the evolution of the sharp contaminant front.

Governing equations and mathematical setup

- The governing equations that describe a multiphase fluid flow in a porous medium in terms of non-aqueous (n), water (w), and air (a) are

$$\frac{\partial}{\partial t}(\rho_n \phi S_n) = \frac{\partial}{\partial x^i}\left[\rho_n \frac{k_{rn}}{\mu_n} k^{ij}\left(\frac{\partial p_a}{\partial x^j} + \rho_n g \frac{\partial z}{\partial x^j}\right)\right] - \frac{\partial}{\partial x^i}\left[\rho_n \frac{k_{rn}}{\mu_n} k^{ij}\left(\frac{\partial p_{can}}{\partial x^j}\right)\right] + q_n, \tag{1}$$

$$\frac{\partial}{\partial t}(\rho_w \phi S_w) = \frac{\partial}{\partial x^i}\left[\rho_w \frac{k_{rw}}{\mu_w} k^{ij}\left(\frac{\partial p_a}{\partial x^j} + \rho_w g \frac{\partial z}{\partial x^j}\right)\right] - \frac{\partial}{\partial x^i}\left[\rho_w \frac{k_{rw}}{\mu_w} k^{ij}\left(\frac{\partial p_{caw}}{\partial x^j}\right)\right] + q_w, \tag{2}$$

$$\frac{\partial}{\partial t}(\rho_a \phi S_a) = \frac{\partial}{\partial x^i}\left[\rho_a \frac{k_{ra}}{\mu_a} k^{ij}\left(\frac{\partial p_a}{\partial x^j} + \rho_a g \frac{\partial z}{\partial x^j}\right)\right] + q_a, \tag{3}$$

where $x^i = (x, y, z)$ are the spatial cartesian coordinates, and t is the time coordinate. ρ_n, ρ_w, ρ_a, $\left[\frac{M}{L^3}\right]$, are the density of the non-aqueous, water, and air, respectively. μ_n, μ_w, μ_a, $\left[\frac{M}{LT}\right]$, are the dynamic viscosity of the non-aqueous, water, and air, respectively. k^{ij} $[L^2]$, g $\left[\frac{L}{T^2}\right]$, z $[L]$, q_α $\left[\frac{M}{L}\right]$, ϕ, are the absolute permeability tensor, the gravity acceleration, the depth, the mass source/sink, and the porosity, respectively. A fourth equation relates the saturation of the different phases and is given by

$$S_w + S_n + S_a = 1. \tag{4}$$

$$p_{caw} = (p_a - p_w), \qquad p_{can} = (p_a - p_n).$$

Governing equations and mathematical setup II

- The PDEs can be written as

$$\frac{\partial \sigma_a}{\partial t} + \frac{\partial \sigma_n}{\partial t} + \frac{\partial \sigma_w}{\partial t} = \phi_0 c_R \frac{\partial p}{\partial t}, \tag{5}$$

$$\begin{aligned} k_{rw} &= S_{ew}^{1/2}[1-(1-S_{ew}^{1/m})^m]^2, \\ k_{ra} &= (1-S_{et})^{1/2}(1-S_{et}^{1/m})^{2m}, \\ k_{rn} &= (S_{et}-S_{ew})^{1/2}[(1-S_{ew}^{1/m})^m-(1-S_{et}^{1/m})^m]^2, \end{aligned}$$

$$S_{et} = \frac{S_w + S_n - S_{wir}}{1 - S_{wir}},$$

$$S_e = [1+\alpha p_c^n]^{(1-\frac{1}{n})},$$

$$\begin{aligned} p_{can} &= -p_{can0}(1-S_{et}^{1/m})^{1-m}, \\ p_{caw} &= -p_{can0}(1-S_{et}^{1/m})^{1-m} - p_{cnw0}(1-S_{ew}^{1/m})^{1-m}. \end{aligned}$$

with

$$\frac{\partial \sigma_{(\alpha)}}{\partial t} = -\frac{\partial}{\partial x^i}\left[F^i_{(\alpha)}(S_w, S_n, S_a, p)\right] + \frac{\partial}{\partial x^i}\left[Q^i_{(\alpha)}(S_w, S_n, S_a, p)\right] \tag{6}$$

and $\alpha = (w, n, a)$:

$$F^i_{(\alpha)}(S_w, S_n, S_a, p) = -\frac{k_{r(\alpha)}(S_w, S_n, S_a)}{\mu_{(\alpha)}} k^{ij}\left(\frac{\partial p}{\partial x^j} + \rho_\alpha g \frac{\partial z}{\partial x^j}\right), \tag{7}$$

does not depend on the spatial derivative of the saturation, and

$$Q^i_{(\alpha)}(S_w, S_n, S_a, p) = -\frac{k_{r(\alpha)}(S_w, S_n, S_a)}{\mu_{(\alpha)}} k^{ij} \frac{\partial p_{ca(\alpha)}(S_w, S_n, S_a)}{\partial x^j}, \tag{8}$$

-

$$\sigma_w \equiv \phi S_w, \sigma_n \equiv \phi S_n, \sigma_a \equiv \phi S_a,$$

High-Resolution Shock-Capturing conservative method

Based of the method presented in Kurganov and Tadmor (KT) J. Comput. Phys. 160, 241–282 (2000)

- The implementation

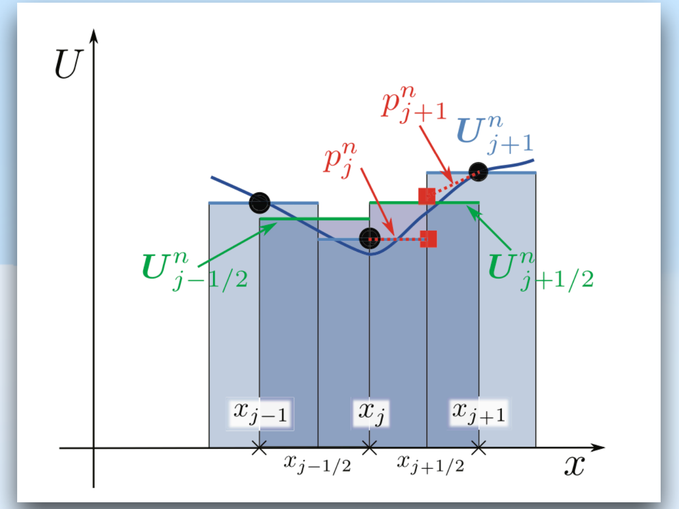

$$\frac{d}{dt}u_j(t) = -\frac{H_{j+1/2}(t) - H_{j-1/2}(t)}{\Delta x} + \frac{P_{j+1/2}(t) - P_{j-1/2}(t)}{\Delta x}$$

$$H_{j+1/2}(t) = -\frac{1}{2}\left[F(u^+_{j+1/2}(t)) + F(u^-_{j+1/2}(t))\right] - \frac{1}{2}a_{j+1/2}(t)\left[u^+_{j+1/2}(t) - u^-_{j+1/2(t)}(t)\right]$$

$$P_{j+1/2}(t) = \frac{1}{2}\left[Q(u_j(t), \frac{u_{j+1}(t) - u_j(t)}{\Delta x}) + Q(u_{j+1}(t), \frac{u_{j+1}(t) - u_j(t)}{\Delta x})\right]$$

- The HRSC method possess the following properties: sharp resolution of discontinuities without considerable smearing; at least second-order of accuracy on smooth parts of the solution; absence of spurious oscillations in the solution; convergence to the “weak” solution as the grid is refined; no use of artificial-viscosity terms. The method belongs to the class of Monotonic Upstream-centered Scheme for Conservation Law (MUSCL).

CactusHydro

High-resolution shock-capturing (HRSC) conservative numerical method applied to groundwater

- To address the shocks front and accurately propagate the front of the fluid component in 3D space and time we use the HRSC conservative method that treats the advective part (hyperbolic) of the PDEs better than other numerical methods when there is a discontinuity since it is a conservative flux method that follows sharp discontinuities accurately and temporal dynamics of three-phase fluid flow in a porous medium.
- The HRSC method has a sharp resolution of the discontinuities without considerable smearing, at least second-order of accuracy on smooth parts of the solution; absence of spurious oscillations in the solution, convergence to the ‘weak’ solution as the grid is refined, no use of artificial viscosity terms.
- The time evolution is performed using a ‘forward’ in time explicit method (instead of a commonly implicit ‘backward’ in time evolution).
- We need High-Performance-Computing (HPC) for parallel, large-scale numerical simulations, creation of distributed data structures, parallelism, I/O, checkpointing, etc.
- **CactusHydro is built up over an open source infrastructure called Cactus** (cactuscode.org)
    - **Cactus is**: a framework for developing portable, modular applications, focusing on HPC.
    - **Cactus was developed for solving computational problems which:**
    - Are too large for single machine
    - Require parallelization (MPI, OpenMP, GPU)
    - Involve multi-physics
    - Use codes written in different programming languages (usa il metodo delle differenze finite).

Anaconda —> for python scripts written for post-processing in data science and matplotlib

HPC @ UNIPR
MARCONI / LEONARDO @ CINECA

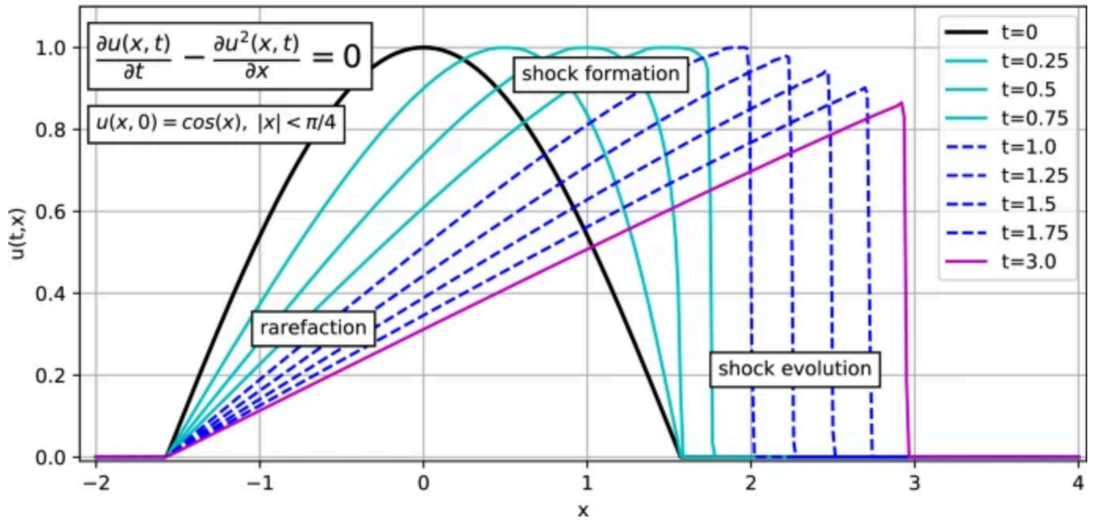

Formation of a shock and rarefaction using the Burgers' equation. The solution at the initial condition for $t = 0$ is represented by a cosine function moving from the left to the right and its time evolution using the HRSC FD method. Notice the formation of a discontinuity jump (shock) and the creation of a rarefaction.

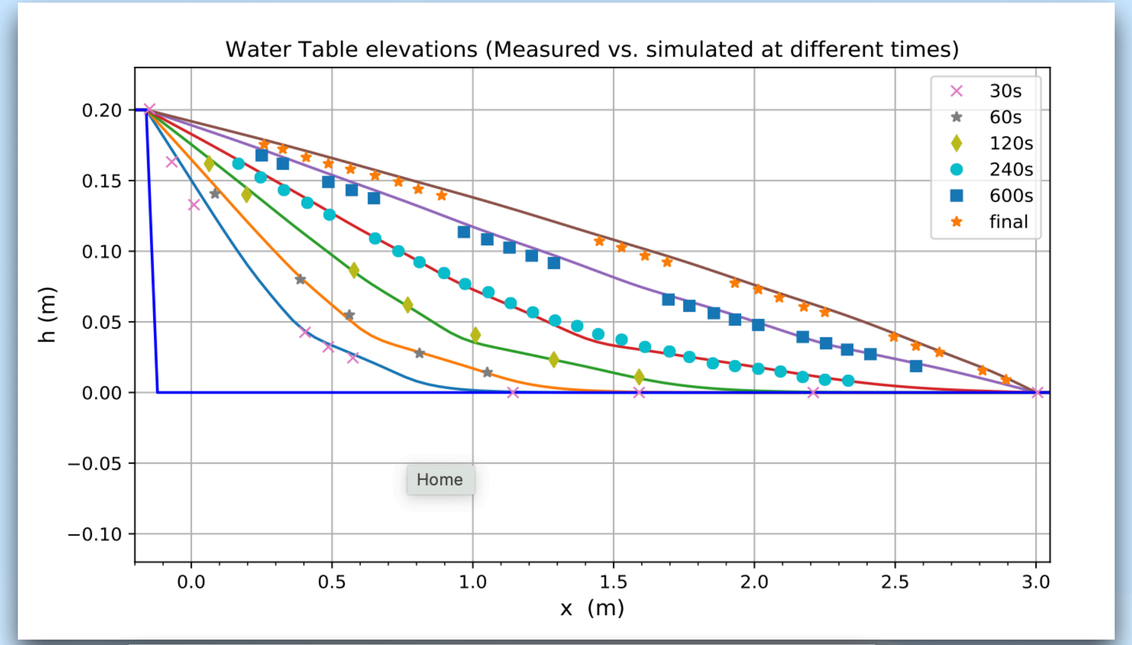

Figure S1. Comparison between the water table elevations, measured in a sand tank experiment [29] (marked colored points), and the corresponding water table elevations computed with CactusHydro (continuum colored line) as a function of the distance, at different times. The numerical results fit very nicely with the experimental one for each time studied. The blue continuum line represents the boundary condition (at t=0 s.). The final line corresponds to a time where the system is already in the final state.

Koichi et al., 1977

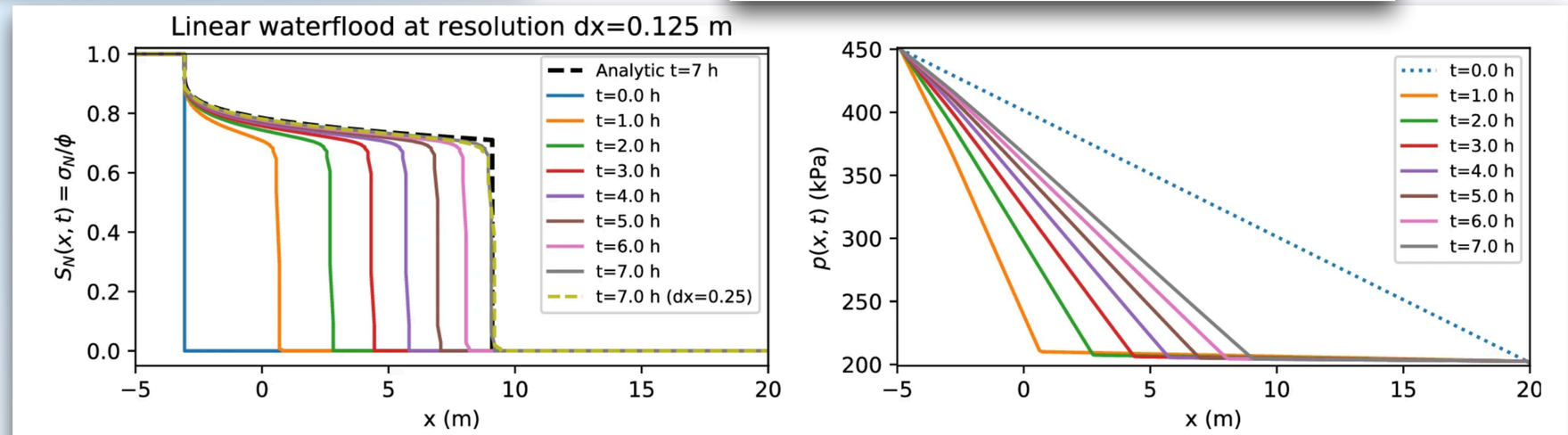

Comparison of NAPL saturation as a function of the distance from NAPL injection and the analytical solution[44] and numerical results from CactusHydro code for a two-phase nonaqueous-water flood.

- List of parameters used for the three-dimensional numerical simulations of LNAPL and DNAPL in variably saturated zones

Parameter	Symbol	Value
Absolute permeability, m^2	k	4.14×10^{-10}
Rock compressibility, Pa^{-1}	c_R	4.35×10^{-7}
Porosity	ϕ_0	0.3
Water viscosity, $kg/(ms)$	μ_w	10^{-3}
Water density, kg/m^3	ρ_w	10^3
Oil viscosity, $kg/(ms)$	μ_n	10^{-1}
Oil density (LNAPL), kg/m^3	ρ_n	881
Oil density (DNAPL), kg/m^3	ρ_n	1200
Air viscosity, $kg/(ms)$	μ_a	0.000018
Air density, kg/m^3	ρ_a	1.225
Van Genuchten parameters	(n, m)	(2,1/2)
Irreducible wetting phase saturation	S_{wir}	0.057
Capillary pressure air-water at zero saturation, m	p_{caw0}	0.081
Capillary pressure air-nonaqueous at zero saturation, m	p_{can0}	0.0566
Resolution, m	$\Delta x = \Delta y = \Delta z$	0.5

3D Numerical Results

Saturation contours of LNAPL (continuous leak, homogeneous aquifer) at different times

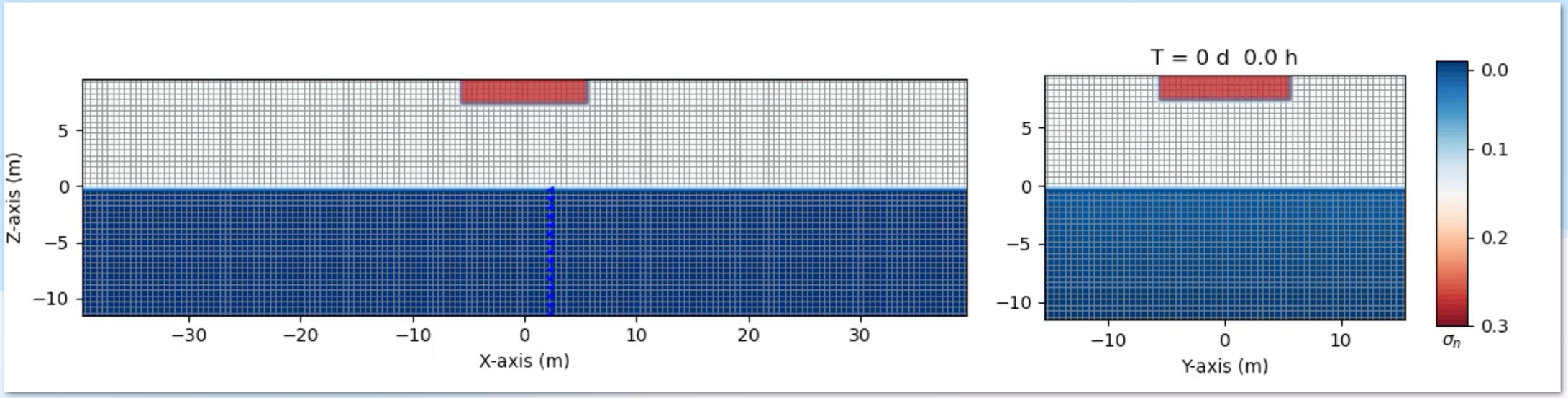

Saturation iso-surface of LNAPL in 3D (generated using VisIt post-processing, open source)

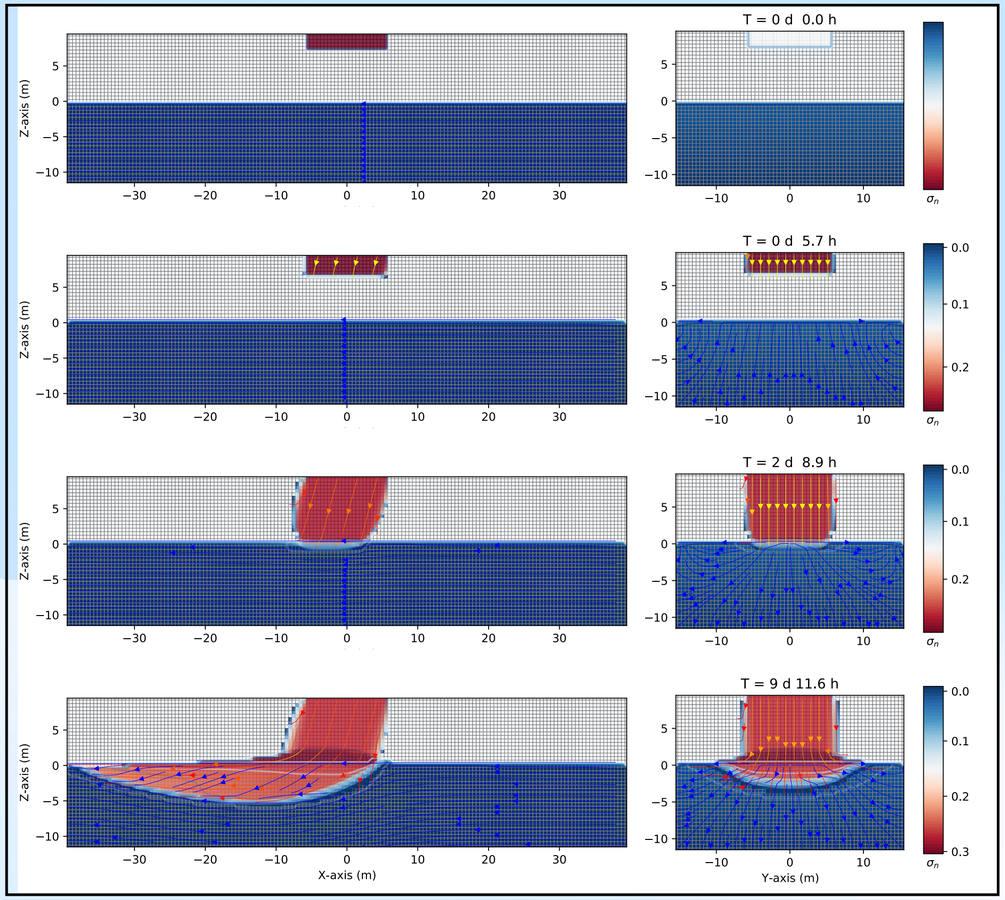

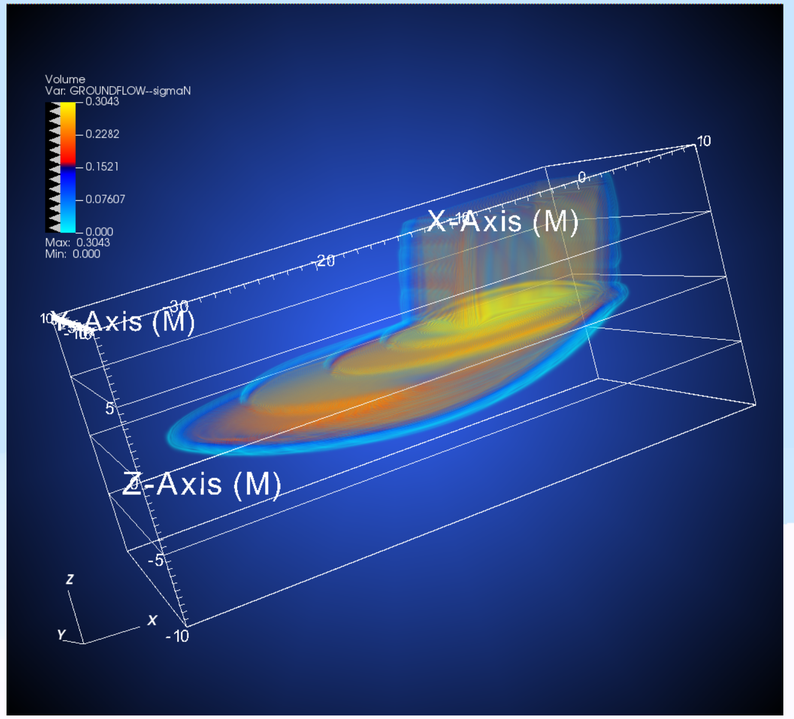

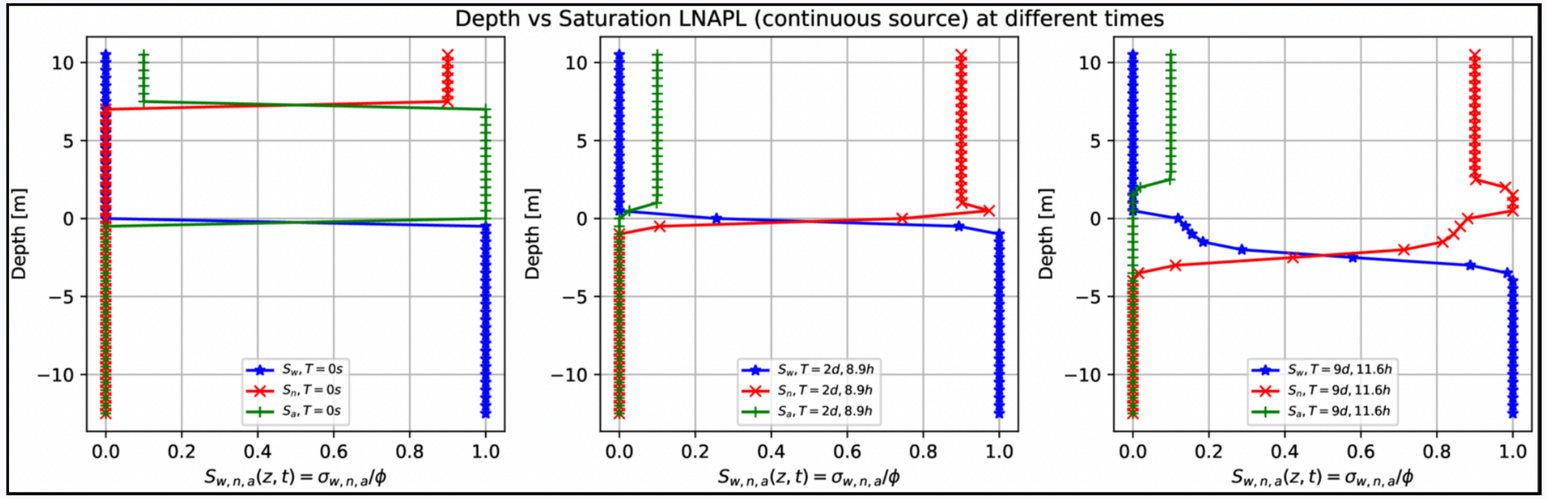

Saturation isocontours of LNAPL (small leak, homogeneous aquifer) at different times

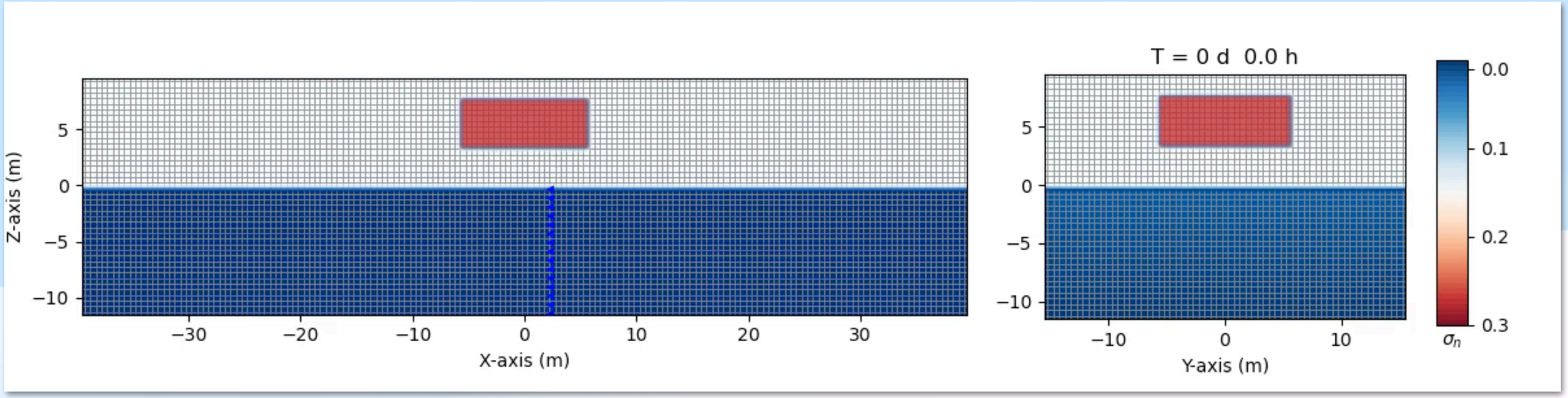

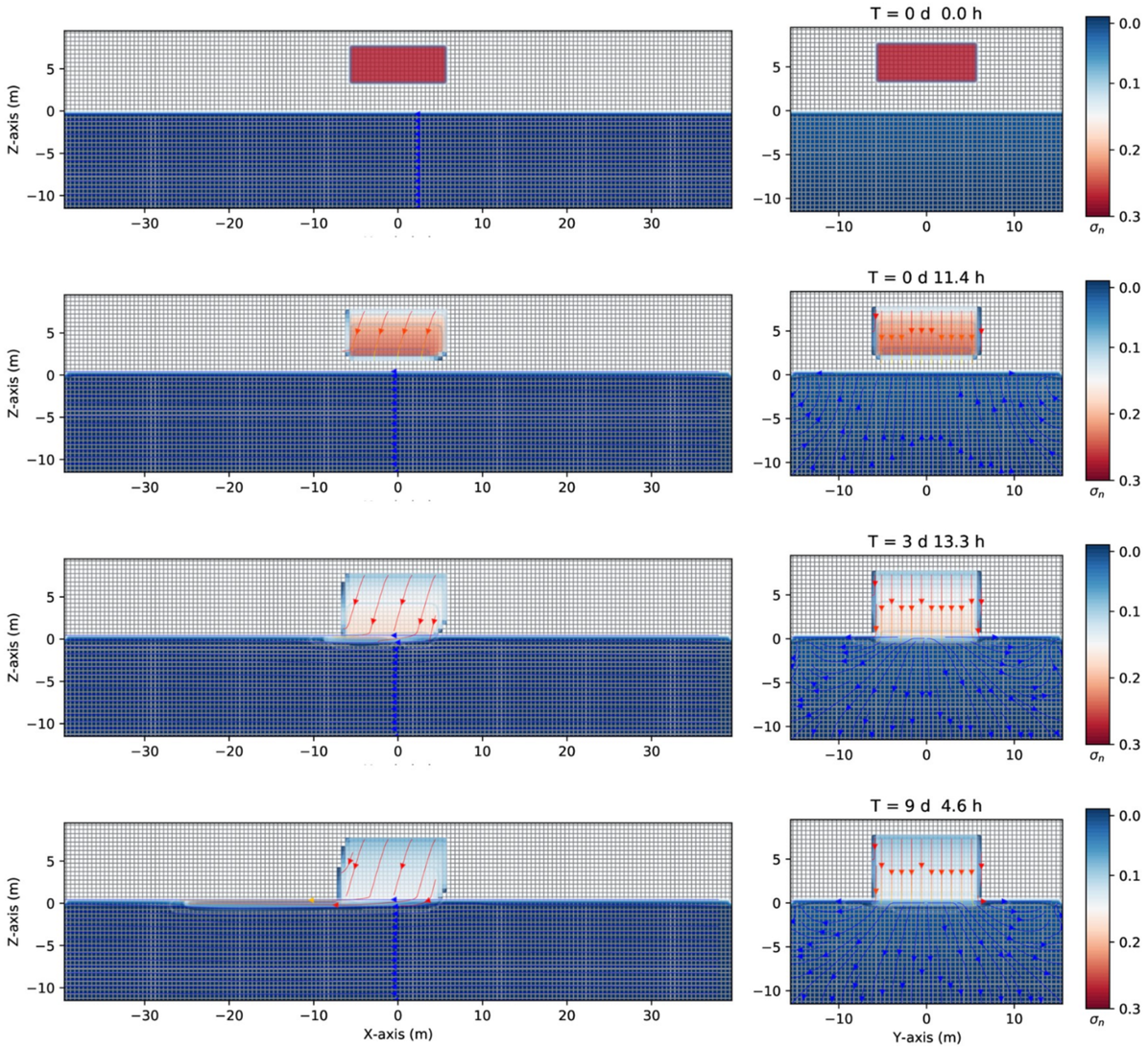

Fig 10. Saturation contours of LNAPL (small source) at different times. Three-dimensional numerical simulation results of the saturation contours ($\sigma_n = S_n\phi$) of a three-phase immiscible fluid flow (water + a small volume source of LNAPL + air) using a spatial grid resolution of 0.50 m and a grid dimension of 80 $m \times 32\ m \times 22\ m$, at different times. Notice how the LNAPL migrates through the saturated zone while moving in the left direction due to a pressure gradient and remains entirely on the capillary fringe zone.

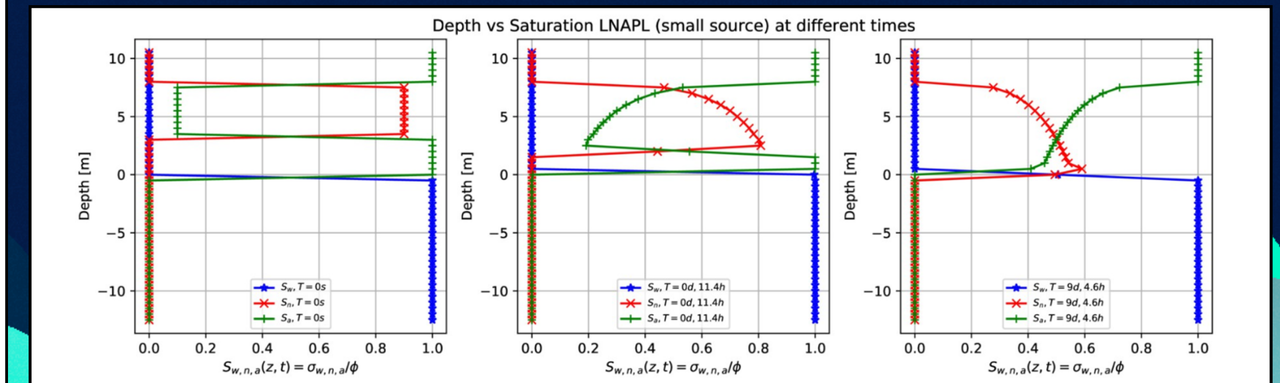

Fig 11. Depth vs. saturation of LNAPL (small source) at different times. Numerical simulation results of a depth as a function of the water saturation S_w (blue points), LNAPL saturation S_n (red points), and air saturation S_a (green points) at various times for a small leak of LNAPL of Fig 10. Initially, at t = 0 s, there is a sharp front of contaminant saturation (red points) situated in the unsaturated zone at z = [4.0,7.0] m. Later, the contaminant moves downward, and the saturation decreases (center). On the right-hand side, the contaminant reaches the groundwater table and does not enter the saturated zone except in a small quantity.

Saturation contours of DNAPL (continuous leak, homogeneous aquifer) at different times

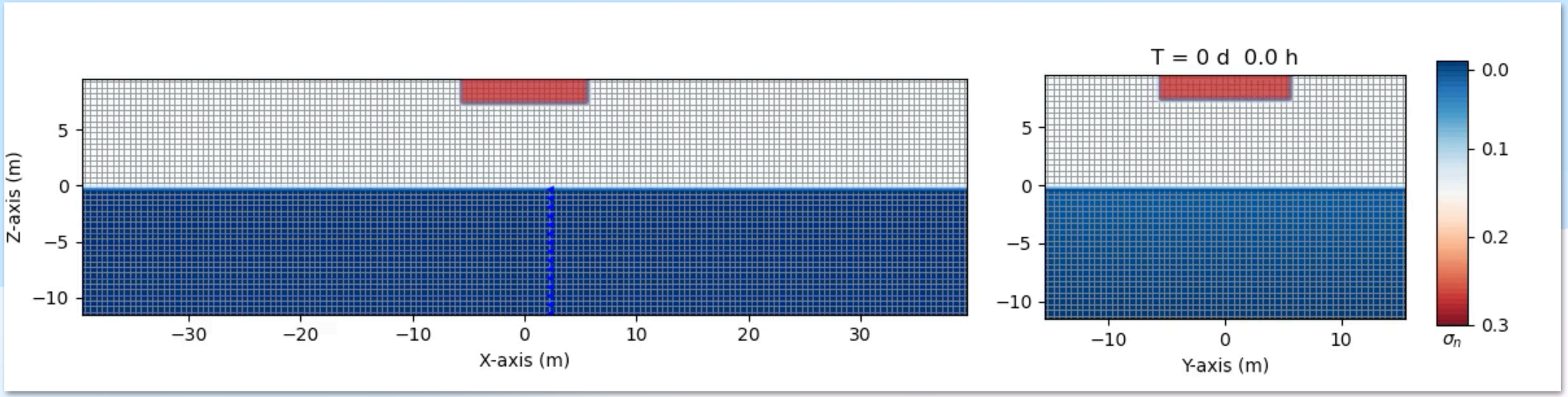

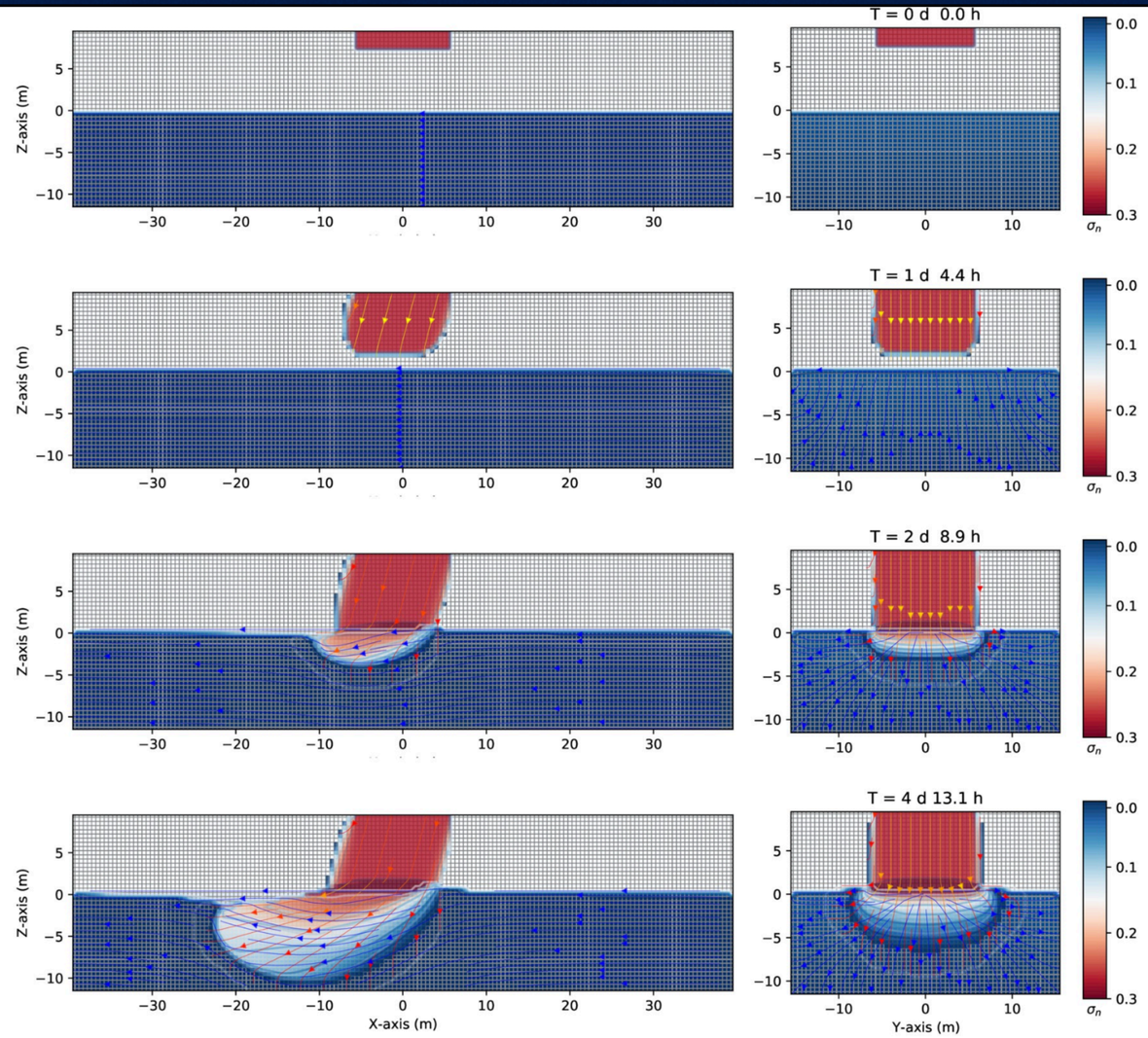

Fig 5. Saturation contours of DNAPL (continuous source) at different times. Three-dimensional numerical simulation results of the saturation contours ($\sigma_n = S_n\phi$) of a three-phase immiscible fluid flow (water + a continuous source of DNAPL + air) using a spatial grid resolution of 0.50 *m* and a grid dimension of 80 *m* × 32 *m* × 22 *m*, at different times. The left-hand side shows the saturation contours in the ($z - x$) plane. The right-hand side shows the saturation contours in the ($z - y$) one. Notice how the DNAPL migrates through the saturated zone while moving in the left direction (where it is positioned a gravity at 15 degrees in the z–x plane, left-hand side). The difference between the previous case (Fig 2) is that now the continuous leak of DNAPL keeps moving to the bottom (aquiclude) of the saturated zone while moving in the left direction due to the pressure gradient.

https://doi.org/10.1371/journal.pone.0266486.g005

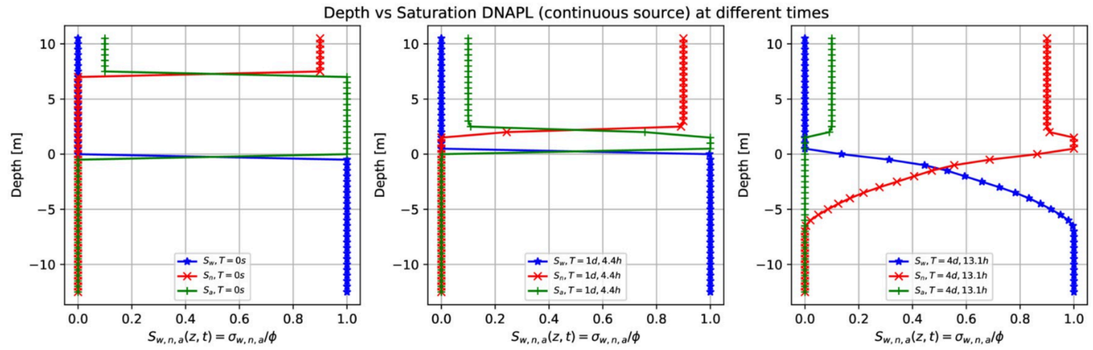

Fig 6. Depth vs. saturation of DNAPL (continuous source) at different times. Three-dimensional numerical simulation results of the depth as a function of the water saturation S_w (blue points), DNAPL saturation S_n (red points), and air saturation S_a (green points) at various times for a continuous leak of DNAPL in Fig 5. Initially, at t = 0 s, a front of contaminant saturation is situated on top of the grid, which rapidly goes to zero. At the same time, it is filled by the air saturation (green point) in the unsaturated zone and water saturation in the saturated one. Notice how the sum of the three-phase saturations is always one. For later times the contaminant (red points) is immersed into the saturated zone.

https://doi.org/10.1371/journal.pone.0266486.g006

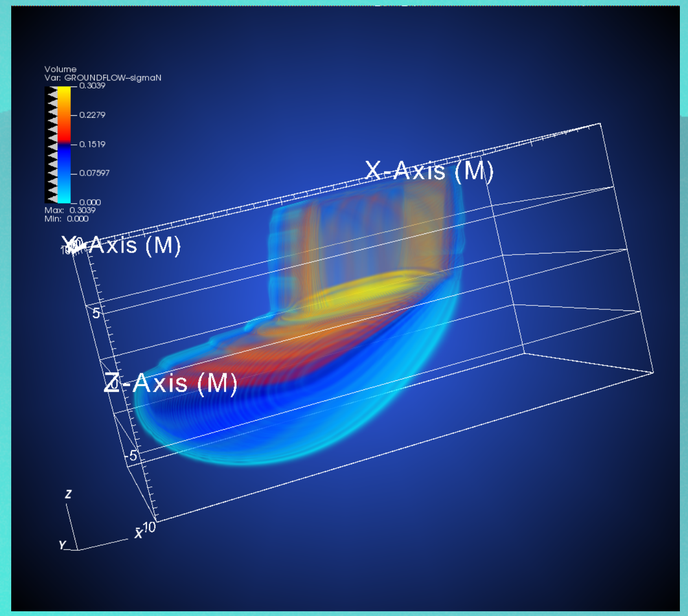

Saturation contours of DNAPL (small leak, homogeneous aquifer) at different times

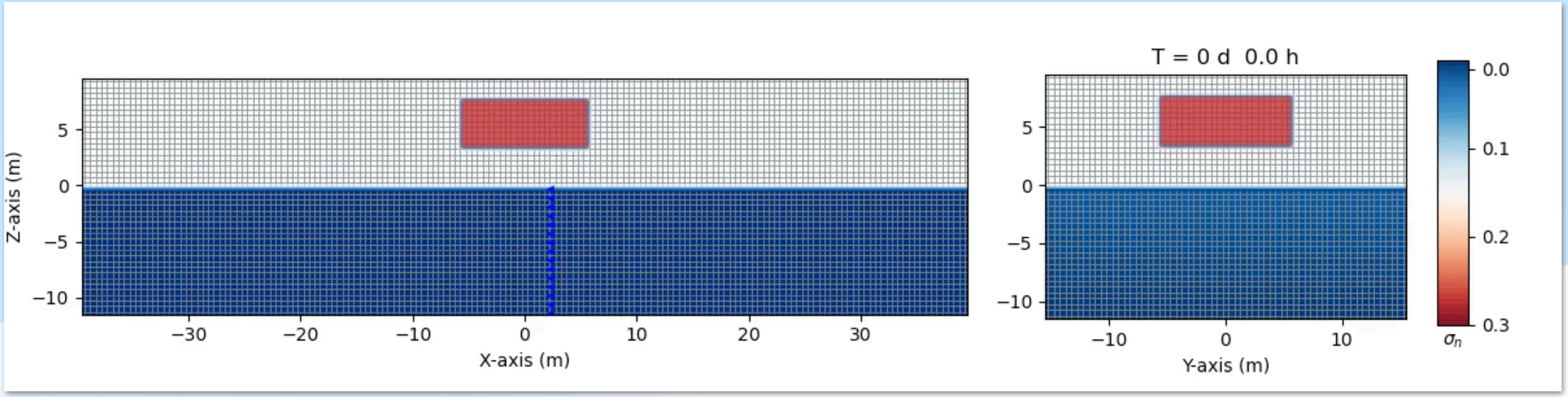

Saturation contours of DNAPL (small leak, homogeneous aquifer) at different times

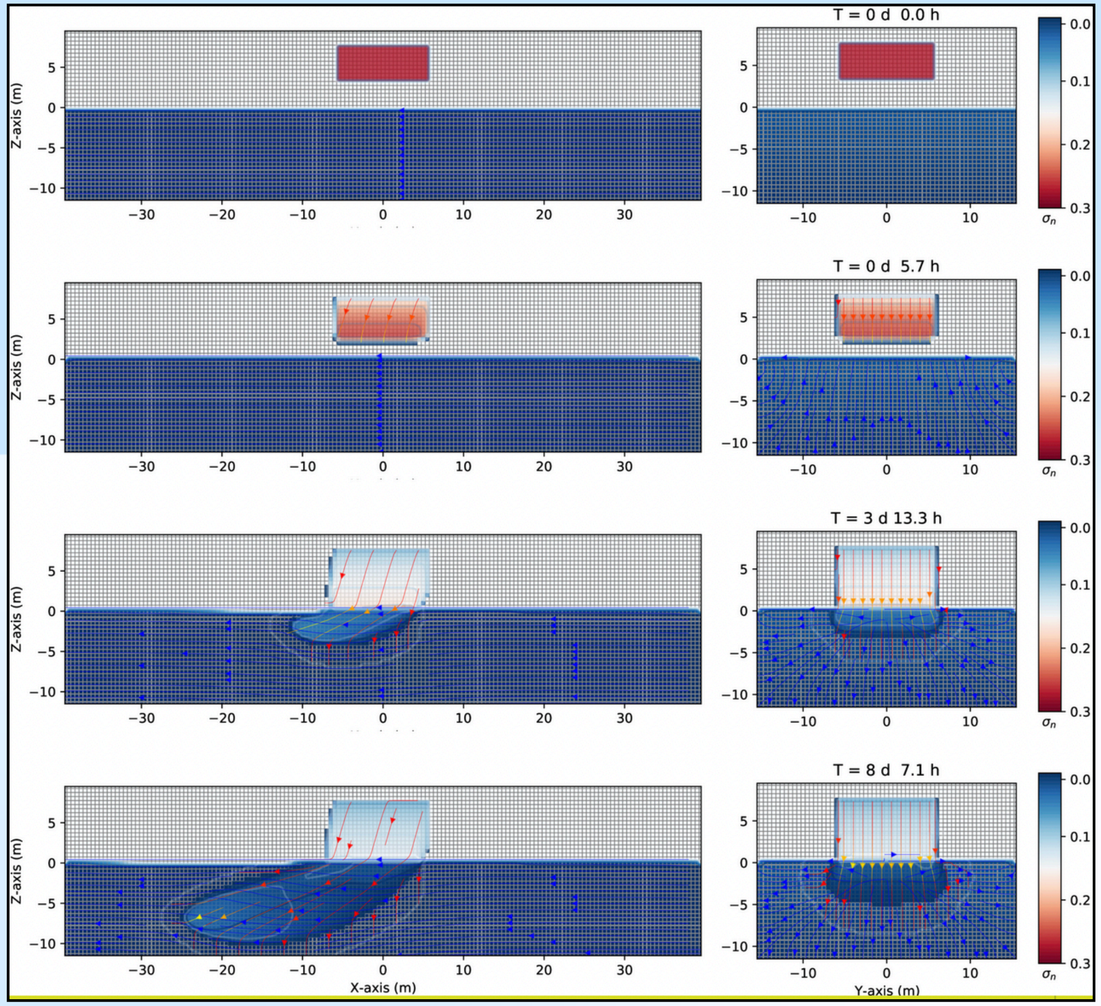

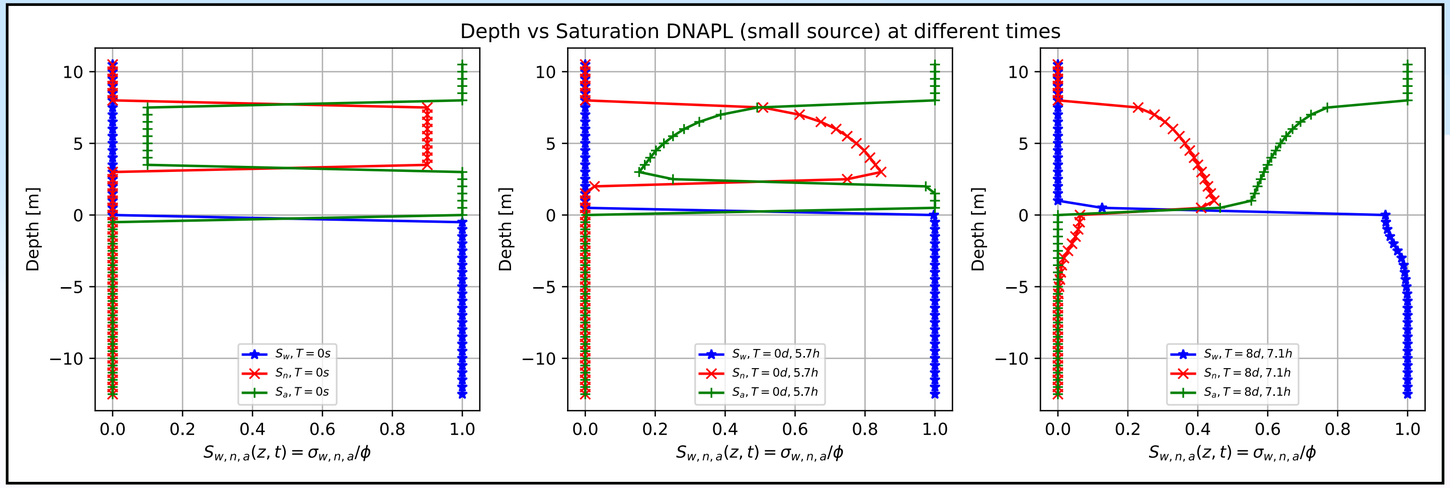

DNAPL (continuous leak, heterogenoeus aquifer and impermeable lenses)

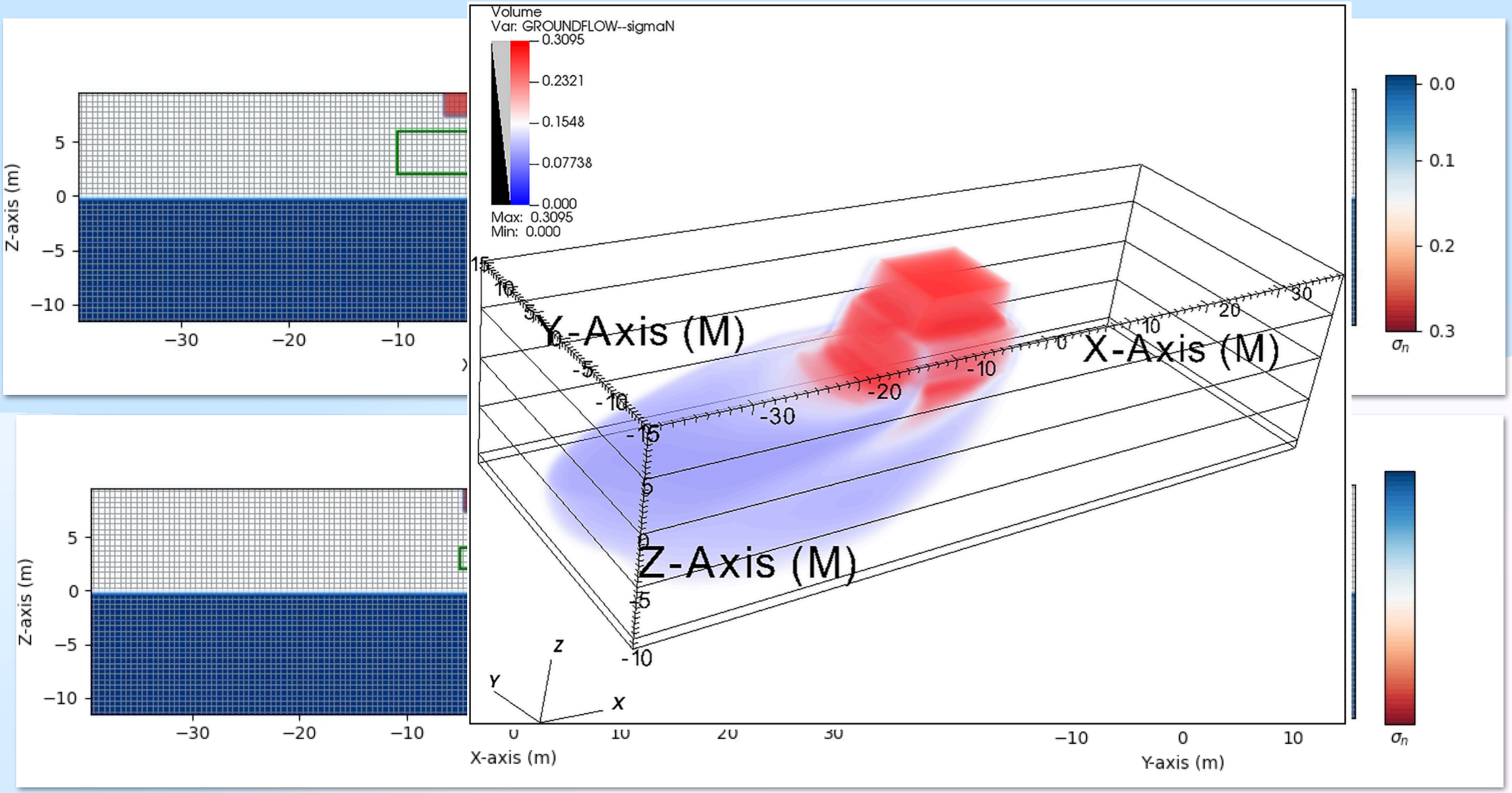

Saturation contours of DNAPL (continuous leak, heterogeneoeus aquifer and impermeable lenses in the saturated zone)

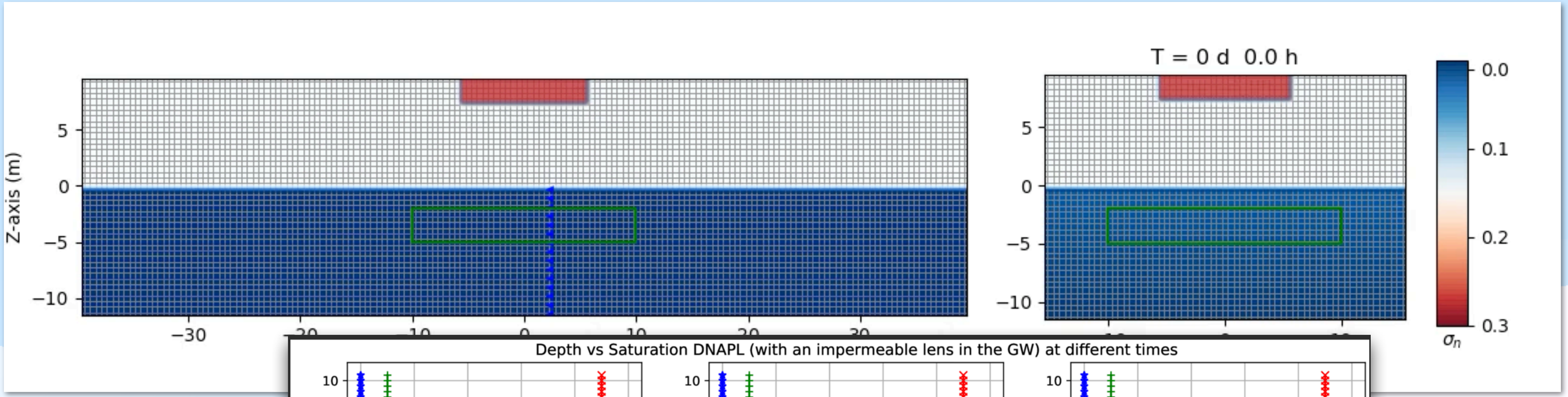

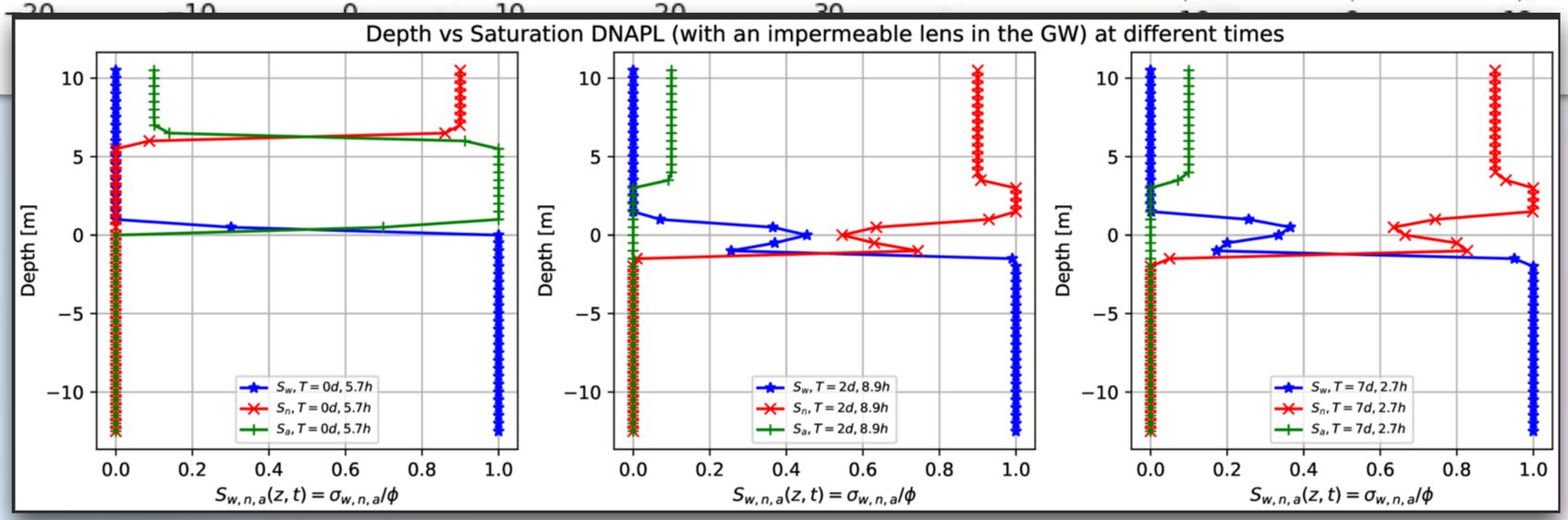

LNAPL application: How to minimise the environmental contamination caused by hydrocarbon releases by onshore pipelines: the key role of a 3D three-phase fluid flow numerical simulation

- We studied the leakage of LNAPL (gasoline or diesel oil), for one hour, from an oil pipeline that comes out with very high pressure (compared to atmospheric pressure) into the surrounding environment. This pipeline is located one meter below the ground surface. Developing a rapid response strategy that might include accurate predictions of oil migration trajectories from numerical simulations modeling is decisive.

Table 1. Definitions of the parameters used in the numerical simulations of a gasoline spill from an oil pipeline.

Parameter	Symbol	Value
Absolute permeability	k	2.059×10^{-11} m^2
Rock compressibility	c_R	4.35×10^{-7} Pa^{-1}
Porosity	ϕ_0	0.43
Water viscosity	μ_w	10^{-3} kg / (ms)
Water density	ρ_w	10^3 kg /m^3
Oil (gasoline) viscosity	μ_n	4.5×10^{-4} kg / (ms)
Oil (gasoline) density	ρ_n	750 kg /m^3
Air viscosity	μ_a	1.8×10^{-5} kg / (ms)
Air density	ρ_a	1.225 kg /m^3
Van Genuchten	(n, m)	$\left(2.68, 1 - \frac{1}{2.68}\right)$
Irreducible wetting phase saturation	S_{wir}	0.045
Superficial tension air-water	σ_{aw}	6.5×10^{-2} N/m
Interfacial tension in nonaqueous water	σ_{nw}	2.6×10^{-2} N/m
Capillary pressure of air-water at zero saturation	p_{caw0}	676.55 Pa
Capillary pressure air-nonaqueous at zero saturation	p_{can0}	405.93 Pa

Table 2. Definitions of the parameters used in the numerical simulations of a diesel oil spill from an oil pipeline.

Parameter	Symbol	Value
Absolute permeability	k	2.059×10^{-11} m^2
Rock compressibility	c_R	4.35×10^{-7} Pa^{-1}
Porosity	ϕ_0	0.43
Water viscosity	μ_w	10^{-3} kg / (ms)
Water density	ρ_w	10^3 kg /m^3
Oil (diesel oil) viscosity	μ_n	3.61×10^{-3} kg / (ms)
Oil (diesel oil) density	ρ_n	830 kg /m^3
Air viscosity	μ_a	1.8×10^{-5} kg / (ms)
Air density	ρ_a	1.225 kg /m^3
Van Genuchten	(n, m)	$\left(2.68, 1 - \frac{1}{2.68}\right)$
Irreducible wetting phase saturation	S_{wir}	0.045
Superficial tension air-water	σ_{aw}	6.5×10^{-2} N/m
Interfacial tension in nonaqueous water	σ_{nw}	3.0×10^{-2} N/m
Capillary pressure of air-water at zero saturation	p_{caw0}	676.55 Pa
Capillary pressure air-nonaqueous at zero saturation	p_{can0}	374.68 Pa

Saturation contours $(\sigma_n = S_n\phi)$ of a three-phase immiscible fluid flow (water, gasoline, air) in a dry soil (Sw=0). The spill is released from the oil pipeline at (x,y,z) = (0,0,1) m and (x,y,z) = (0,0,10) m

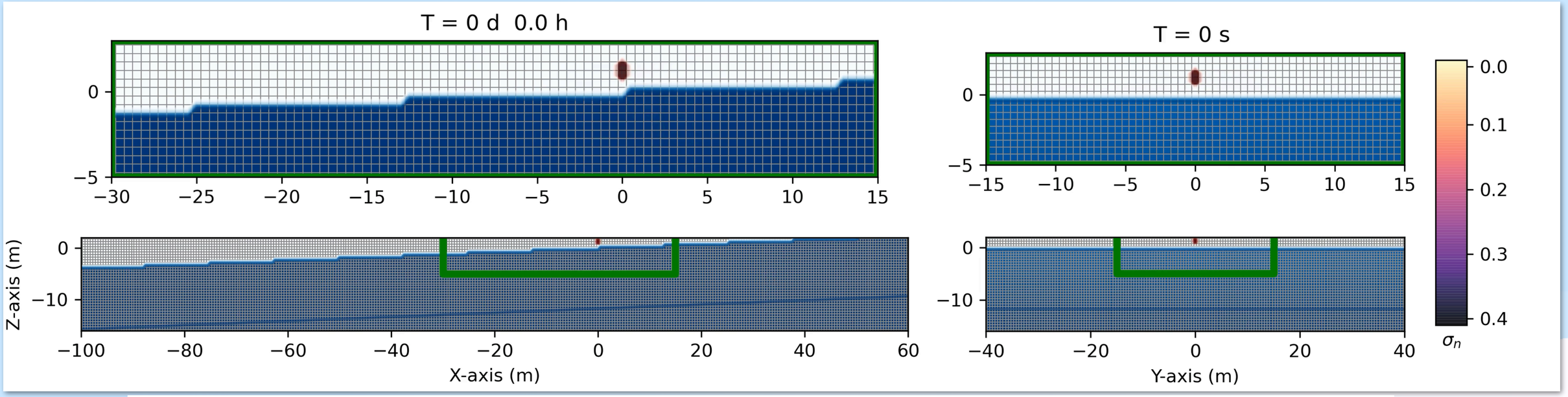

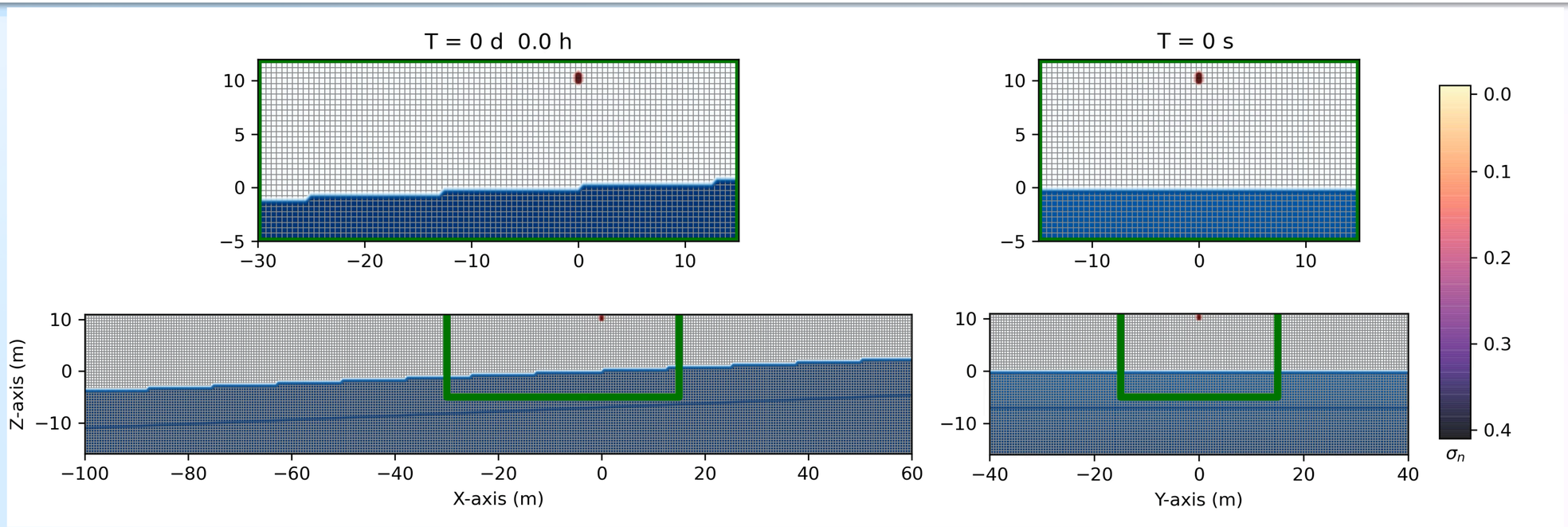

Figure 4. Three-dimensional numerical results on the saturation contours ($\sigma_n = S_n\phi$) of a three-phase immiscible fluid flow (water, gasoline, and air) in a dry soil using a spatial grid resolution of 0.50 m and a grid dimension of 160 × 80 × 18 m, at different times: (**a**) t = 0 s; (**b**) t = 204 s; (**c**) t = 102,400 s; (**d**) t = 2,080,768 s. A hydraulic gradient of 0.04. Left-hand side shows the saturation contours in the $(z - x)$ plane. Right-hand side shows the saturation contours on the $(y - x)$ one. The spill is released from an oil pipeline at $(x, y, z) = (0, 0, 1)$ m.

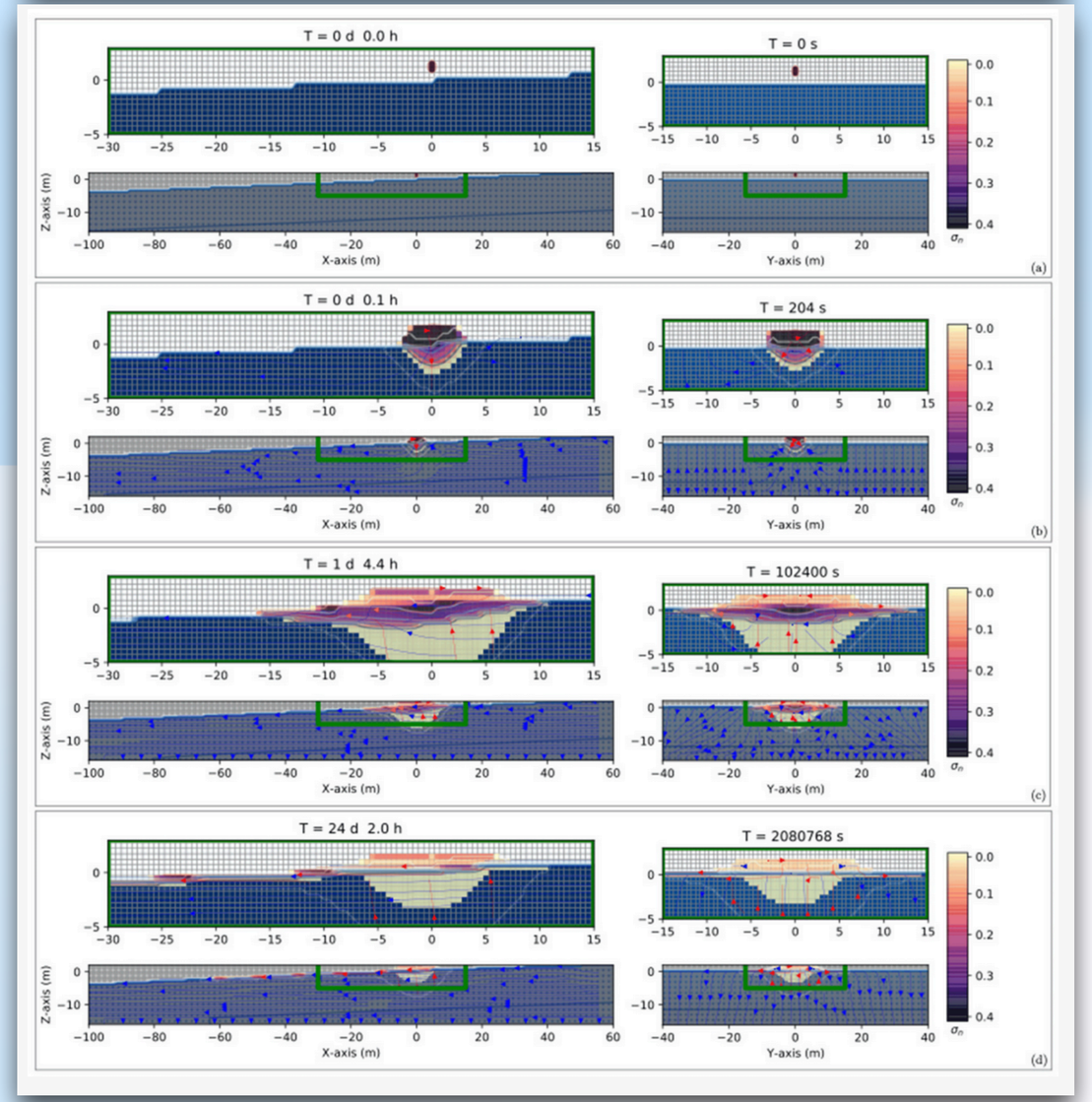

Figure 6. Three-dimensional numerical results on the saturation contours ($\sigma_n = S_n\phi$) of a three-phase immiscible fluid flow (water, gasoline, and air) in a dry soil using a spatial grid resolution of 0.50 m and a grid dimension of 160 × 80 × 27 m, at different times: (**a**) t = 3686 s; (**b**) t = 7168 s; (**c**) t = 102,400 s; (**d**) t = 1,040,998 s. A hydraulic gradient of 0.04. The spill is released from an oil pipeline at $(x, y, z) = (0, 0, 10)$ m. Notice that the first panel corresponds to a time equal to 3686 s rather than the initial time equal to zero.

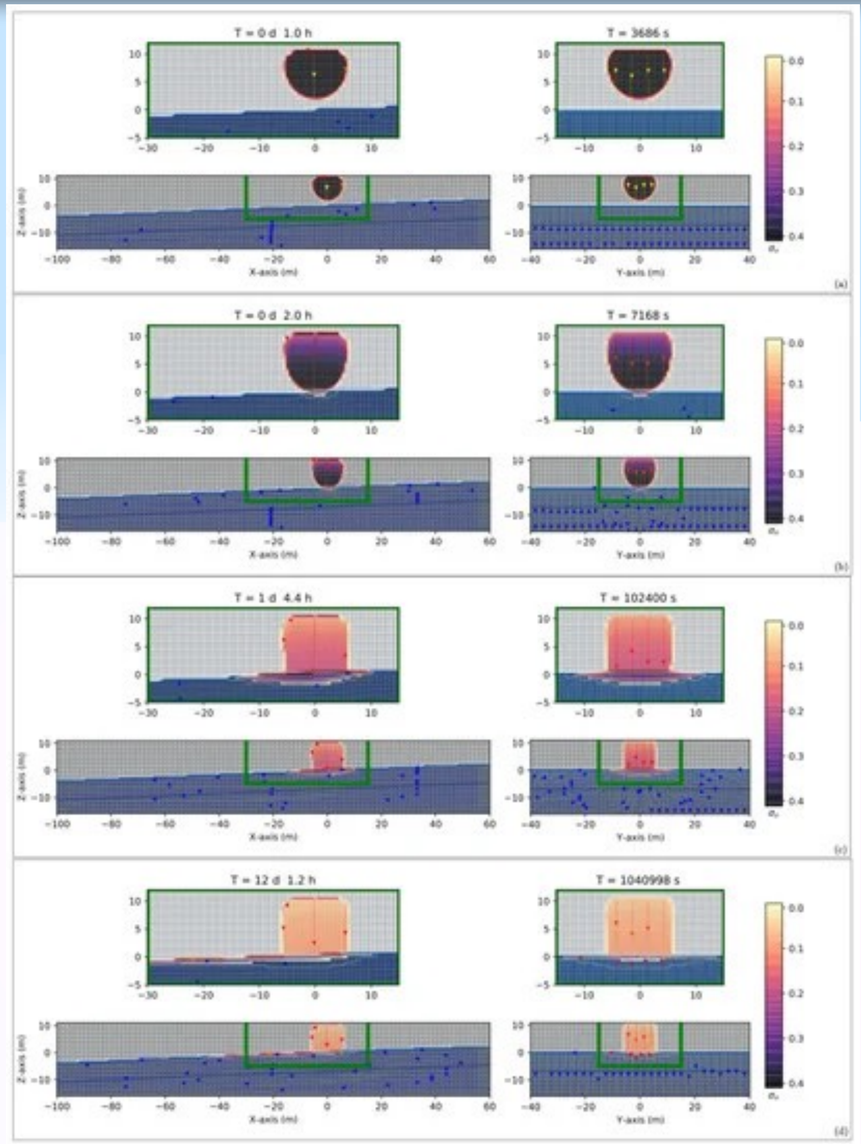

Saturation contours $(\sigma_n = S_n\phi)$ of a three-phase immiscible fluid flow (water, gasoline, air) in an unsaturated zone with Sw=0.20. The spill is released from the oil pipeline at (x,y,z) = (0,0,1) m and (x,y,z) = (0,0,10) m.

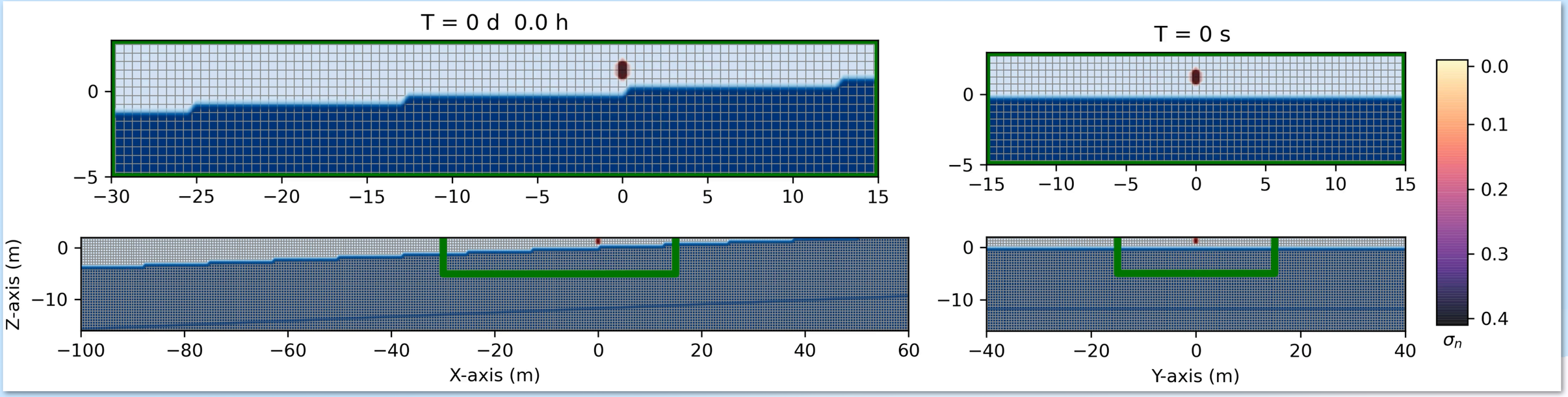

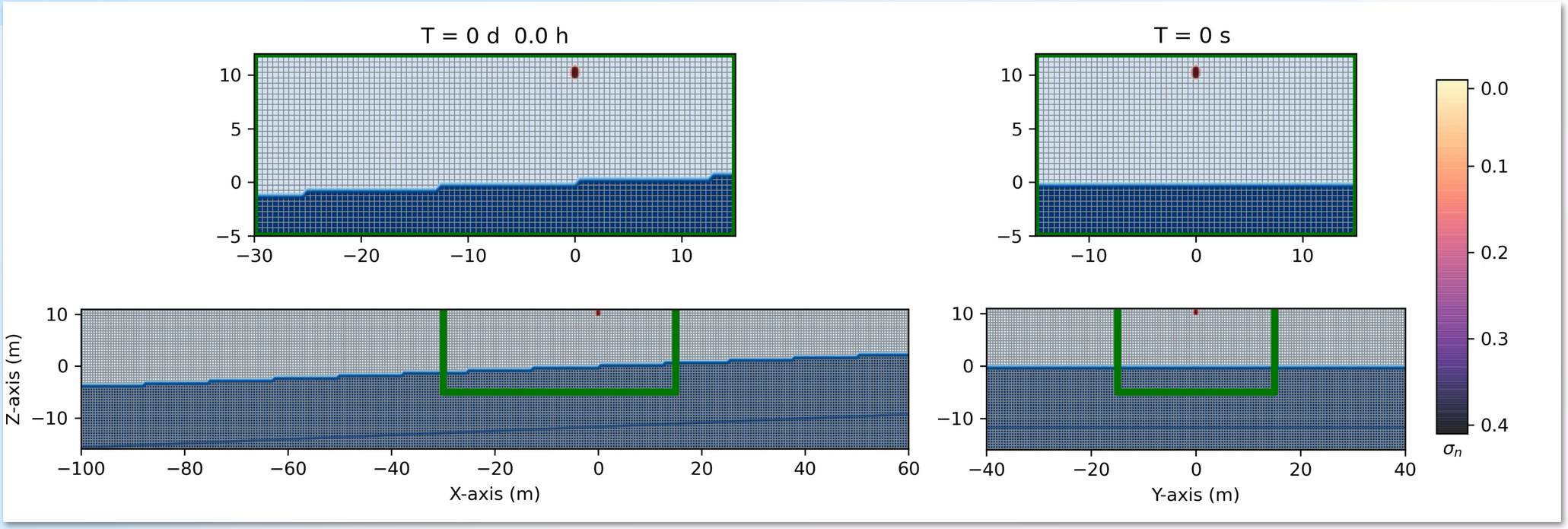

Figure 8. Three-dimensional numerical results on the saturation contours $(\sigma_n = S_n\phi)$ of a three-phase immiscible fluid flow (water, gasoline, and air) using a spatial grid resolution of 0.50 m and a grid dimension of 160 × 80 × 18 m, at different times: (**a**) t = 0 s; (**b**) t = 204 s; (**c**) t = 102,400 s; (**d**) t = 482,508 s. A hydraulic gradient of 0.04. The spill was released from an oil pipeline at $(x, y, z) = (0, 0, 1)$ m. The unsaturated zone has a $S_w = 0.20$.

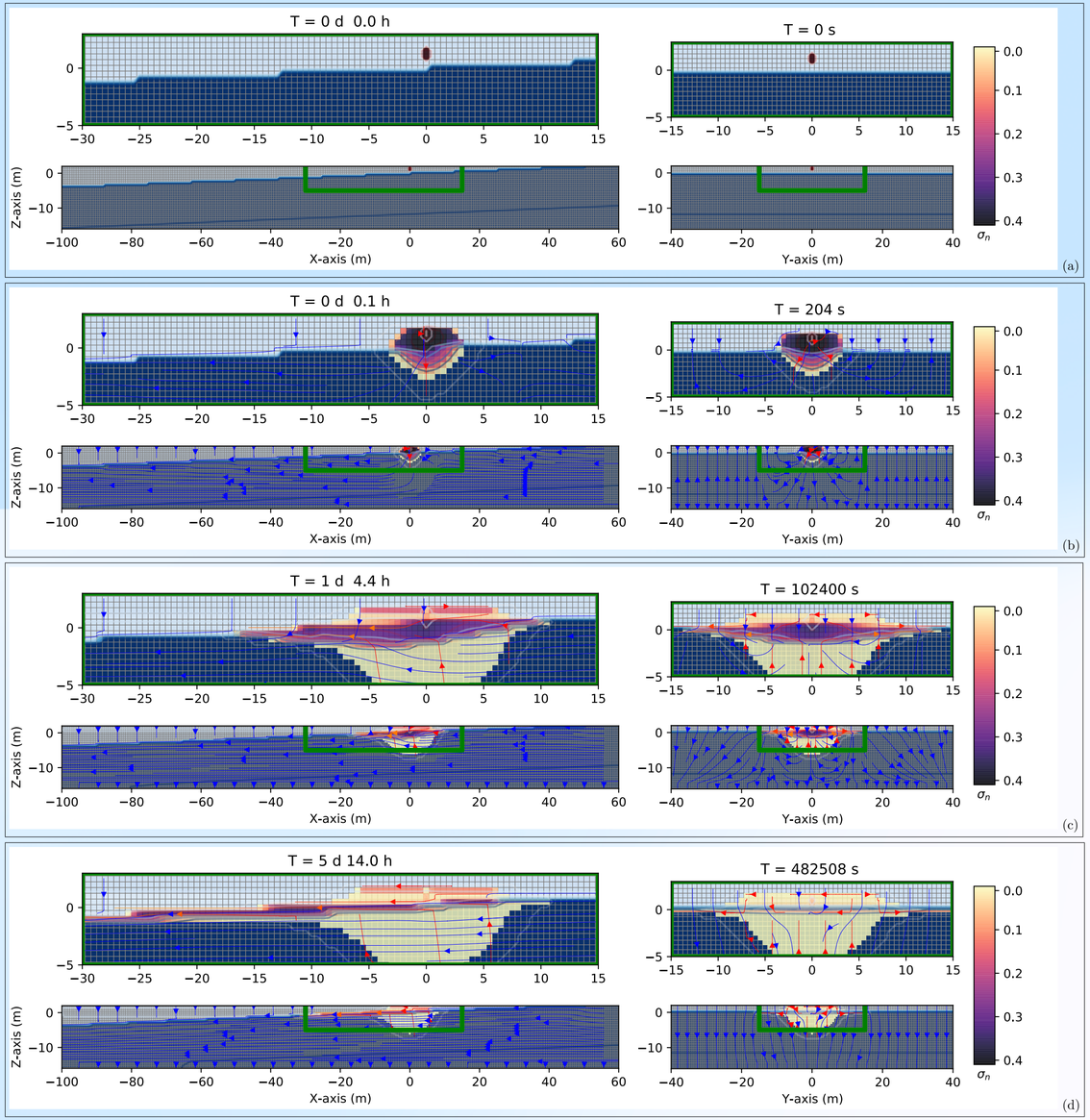

Figure 10. Three-dimensional numerical results on the saturation contours $(\sigma_n = S_n\phi)$ of a three-phase immiscible fluid flow (water, gasoline, and air) using a spatial grid resolution of 0.50 m and a grid dimension of 160 × 80 × 27 m, at different times: (**a**) t = 1228 s; (**b**) t = 3686 s; (**c**) t = 102,400 s; (**d**) t = 285,900 s. A hydraulic gradient of 0.04. The spill was released from an oil pipeline at $(x, y, z) = (0, 0, 10)$ m. The unsaturated zone has a $S_w = 0.20$.

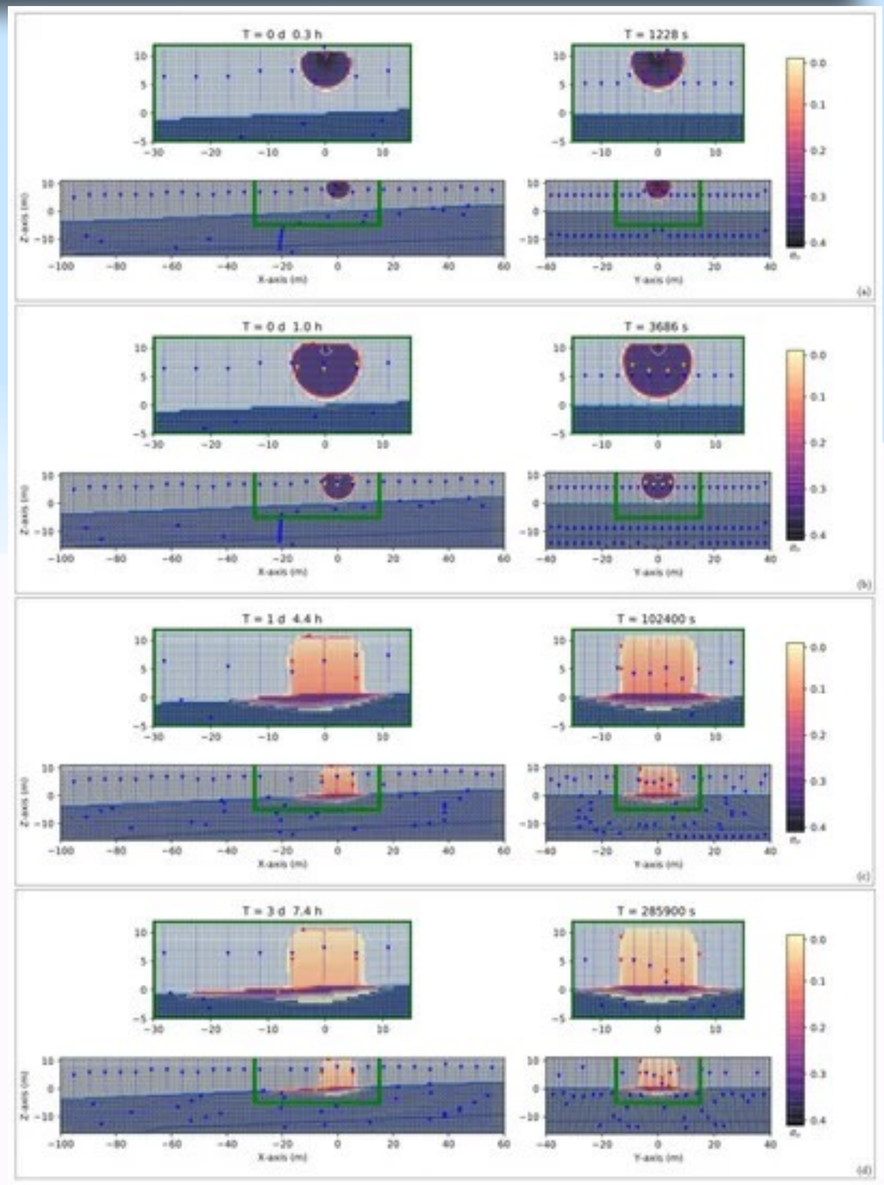

Saturation contours $(\sigma_n = S_n\phi)$ of a three-phase immiscible fluid flow (water, gasoline, air) in an unsaturated zone with Sw=0.50. The spill is released from the oil pipeline at (x,y,z) = (0,0,1) m and (x,y,z) = (0,0,10) m.

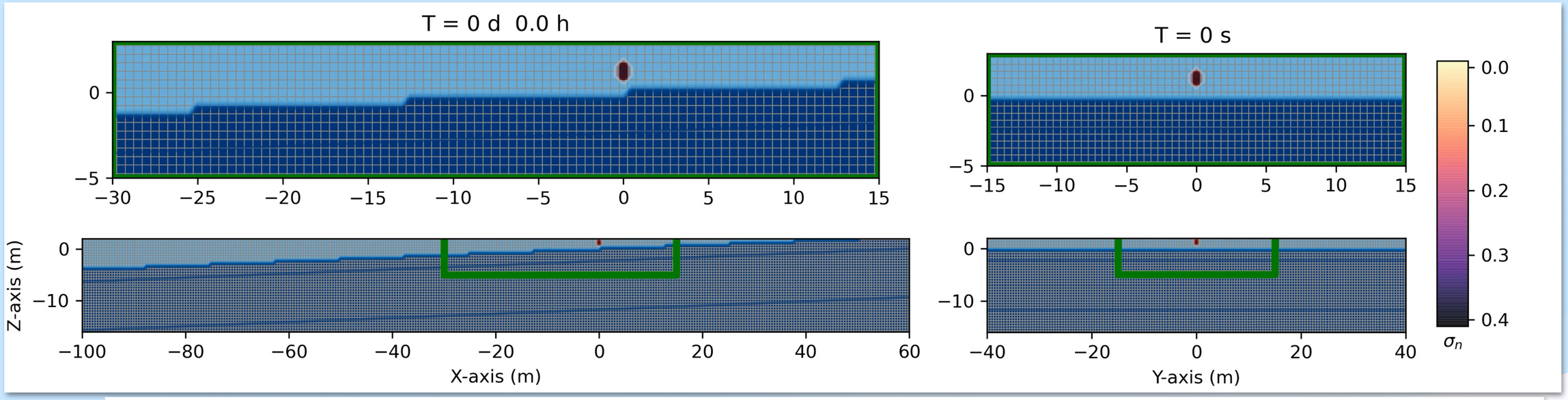

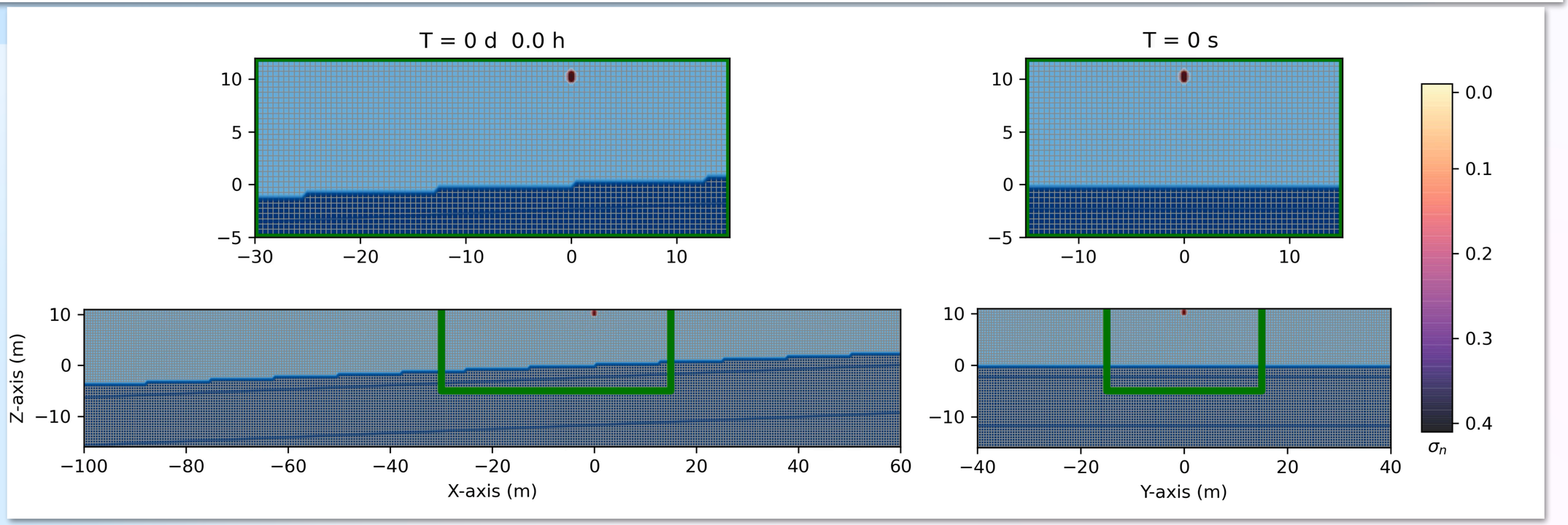

Figure 9. Three-dimensional numerical results on the saturation contours $(\sigma_n = S_n\phi)$ of a three-phase immiscible fluid flow (water, gasoline, and air) using a spatial grid resolution of 0.50 m and a grid dimension of 160 × 80 × 18 m, at different times: (**a**) t = 0 s; (**b**) t = 204 s; (**c**) t = 102,400 s; (**d**) t = 409,600 s. A hydraulic gradient of 0.04. The spill was released from an oil pipeline at $(x, y, z) = (0, 0, 1)$ m. The unsaturated zone has a $S_w = 0.50$.

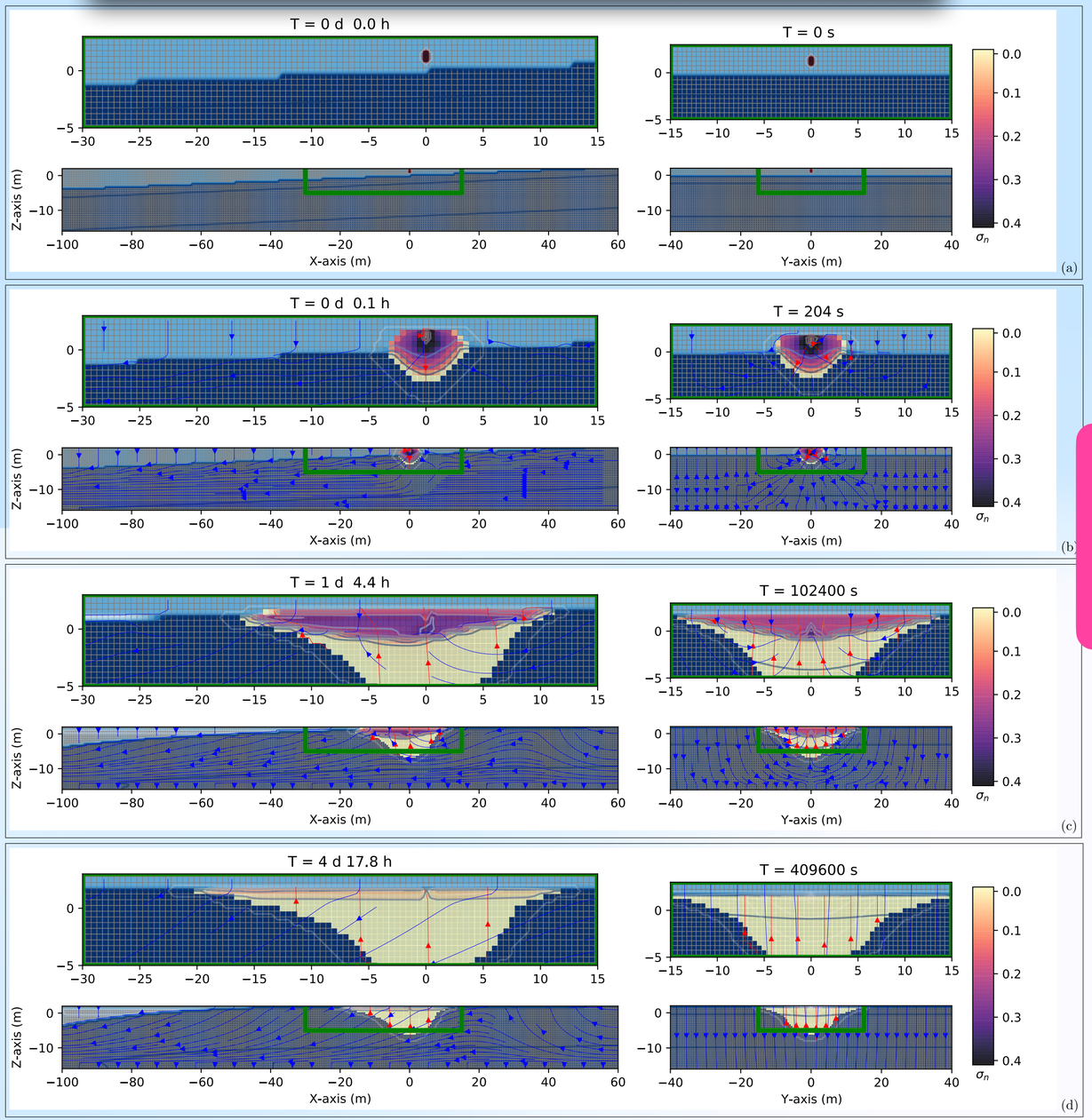

Figure 11. Three-dimensional numerical results on the saturation contours $(\sigma_n = S_n\phi)$ of a three-phase immiscible fluid flow (water, gasoline, and air) using a spatial grid resolution of 0.50 m and a grid dimension of 160 × 80 × 27 m, at different times: (**a**) t = 204 s; (**b**) t = 3686 s; (**c**) t = 102,400 s; (**d**) t = 301,875 s. A hydraulic gradient of 0.04. The spill was released from an oil pipeline at $(x, y, z) = (0, 0, 10)$ m. The unsaturated zone has a $S_w = 0.50$.

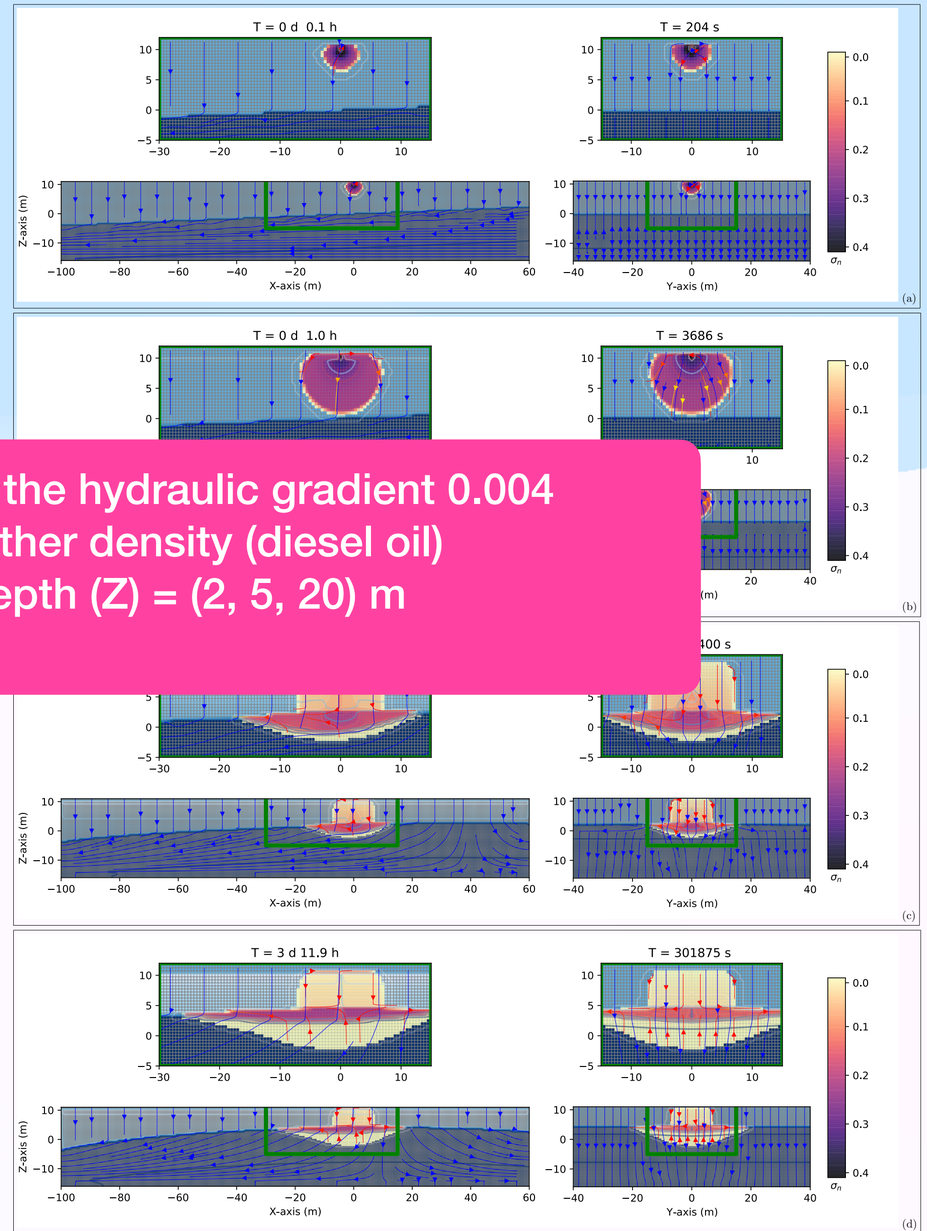

Analysed the hydraulic gradient 0.004
Another density (diesel oil)
Depth (Z) = (2, 5, 20) m

Effects on the density of the contaminant

Table 3. Analysis of arrival time at the groundwater table and the position in the x coordinate under different parameter conditions: two different densities, two different hydraulic gradients, and five different depths from the oil pipeline spill and dry soil. The "-" sign indicates no available results, i.e., the contaminant is still moving in the unsaturated zone and has not reached the groundwater table.

Type (Density)	Thickness of the Unsaturated Zone (m)	Hydraulic Gradient	Arrival Time at the Groundwater Table (s)	Position in *x* after One Day and 4.4 h (m)
Gasoline	1.0	0.04	≤ 204.8	−16.0
		0.004	≤ 204.8	−14.0
Diesel oil	1.0	0.04	≤ 204.8	−6.0
		0.004	≤ 204.8	−5.5
Gasoline	2.0	0.04	≤ 204.8	−16.5
		0.004	≤ 204.8	−15.0
Diesel oil	2.0	0.04	614.4	−6.0
		0.004	614.4	−5.0
Gasoline	5.0	0.04	1228.8	−16.5
		0.004	1228.8	−15.0
Diesel oil	5.0	0.04	10,854.4	−3.5
		0.004	12,288.0	−3.5
Gasoline	10.0	0.04	6348.8	−14.0
		0.004	6348.8	−12.5
Diesel oil	10.0	0.04	286,720.0	-
		0.004	276,480.0	-
Gasoline	20.0	0.04	92,160.0	−2.5
		0.004	92,160.0	−2.5
Diesel oil	20.0	0.04	-	-
		0.004	-	-

Figure 18. Depth versus arrival time at the groundwater table for dry soil, for two different LNAPLs. The data was taken from the numerical simulations of the saturation contours previously shown in **Table 3**.

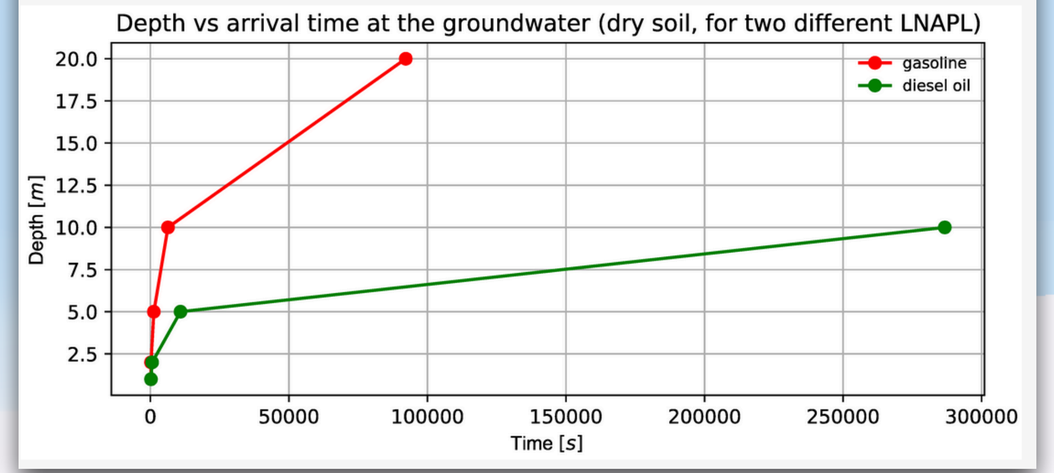

Effects on the water saturation of the unsaturated zone

Table 4. Analysis of arrival time at the groundwater table and the position in the x coordinate under different parameter conditions: two different types of densities, two different depths from the oil pipeline spill and, water saturation of the unsaturated zone equal to 0.20 and 0.50. The hydraulic gradient is 0.04.

Unsaturated Zone Depth (m)	Type of Contaminant	Water Saturation in the Unsaturated Zone	Arrival Time of to the Groundwater Table (s)	Position in *x* after 1 Day and 4.4 h (s)
		0.0	≤ 204.8	−16.0
1.0	Gasoline	0.2	≤ 204.8	−16.0
		0.5	≤ 204.8	−16.0
		0.0	≤ 204.8	−6.0
1.0	Diesel oil	0.2	≤ 204.8	−6.0
		0.5	≤ 204.8	−6.0
		0.0	6348.8	−14.0
10.0	Gasoline	0.2	4915.0	−16.0
		0.5	4710.4	−16.0
		0.0	286,720.0	-
10.0	Diesel oil	0.2	151,552.0	-
		0.5	73,720.0	−1.5

Figure 19. Water saturation in the unsaturated zone versus arrival time at the groundwater table, for two different species of LNAPL. Red line corresponds to gasoline and green line corresponds to diesel oil.

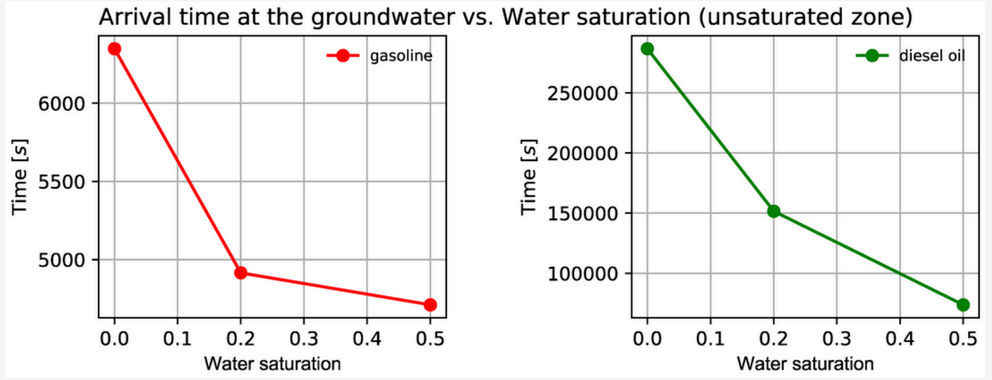

Effects on pressure in the oil pipeline

Table 5. Water saturation of the unsaturated zone vs. arrival time at the groundwater table for a gasoline spill at the atmospheric pressure.

Unsaturated Zone Depth (m)	Type of Contaminant	Water Saturation in the Unsaturated Zone	Arrival Time at the Groundwater Table (s)
1.0	Gasoline	0.0	1024.0
1.0	Gasoline	0.20	819.2
1.0	Gasoline	0.50	614.4

the spill pressure is 2.0×10^6 Pa

Figure 20. Arrival time at the groundwater table vs. water saturation of the unsaturated zone for two different pressure spills of the gasoline.

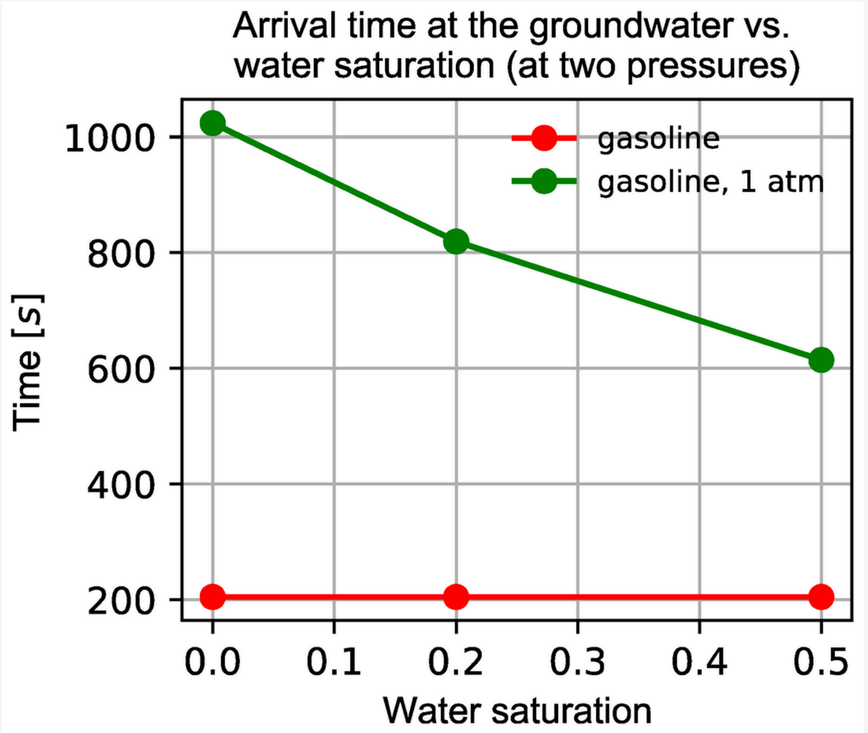

Crude Oil (Petroleum) at 2 meters from the GW

Crude oil density	ρ_n	831.8 kg/m^3
Crude oil dynamics viscosity	μ_n	3.107 $kg/(ms)$

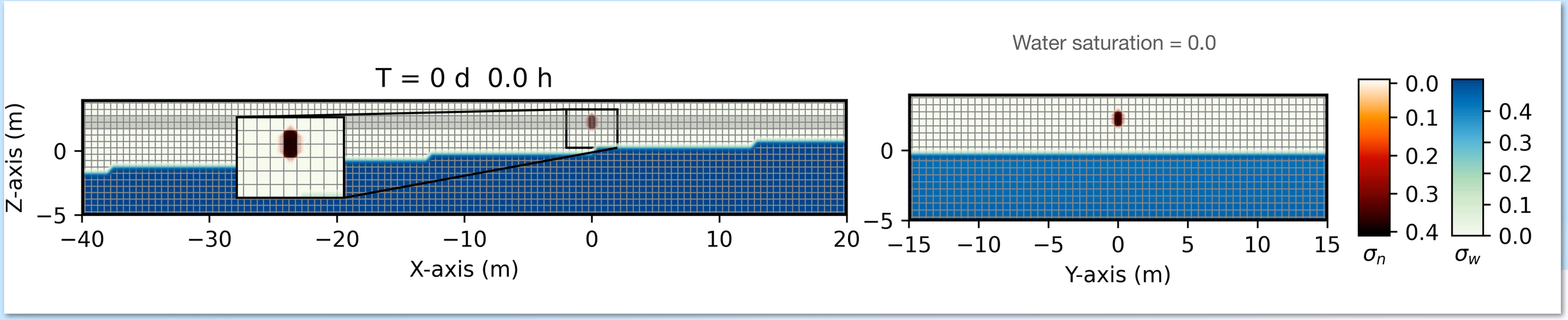

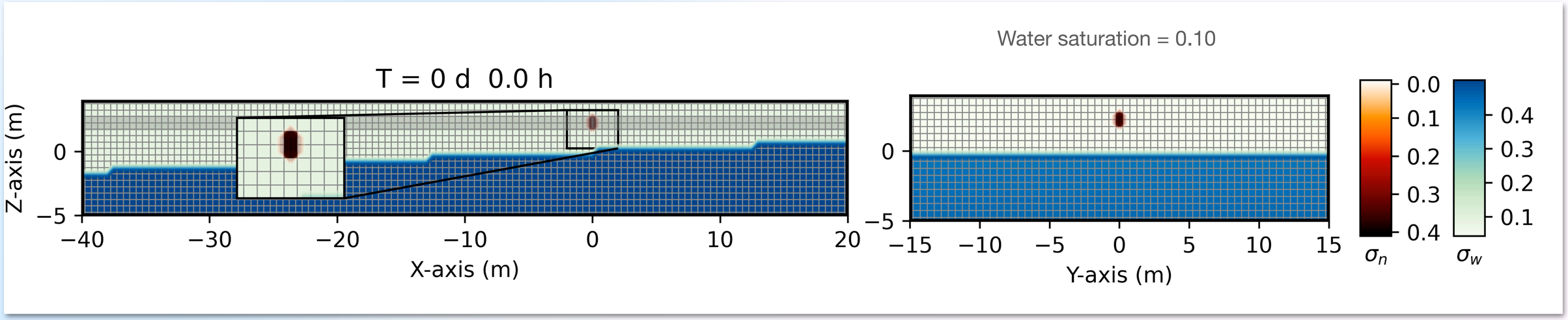

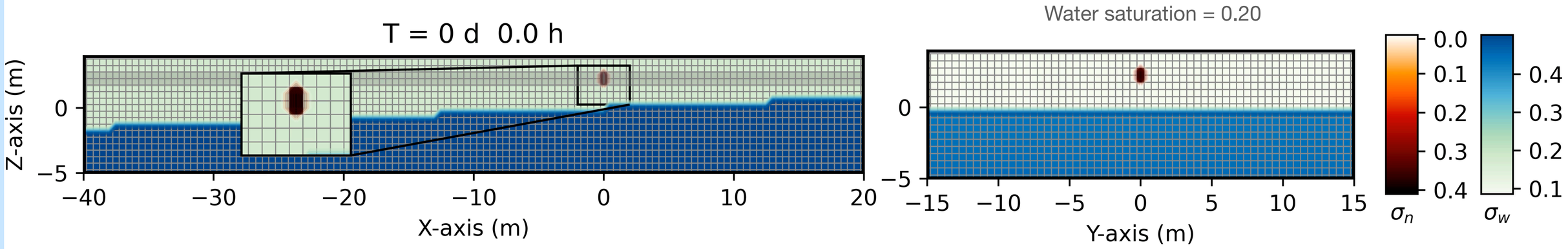
T = 0 d 0.0 h
Z-axis (m)
X-axis (m)
Water saturation = 0.20
Y-axis (m)
σ_n
σ_w

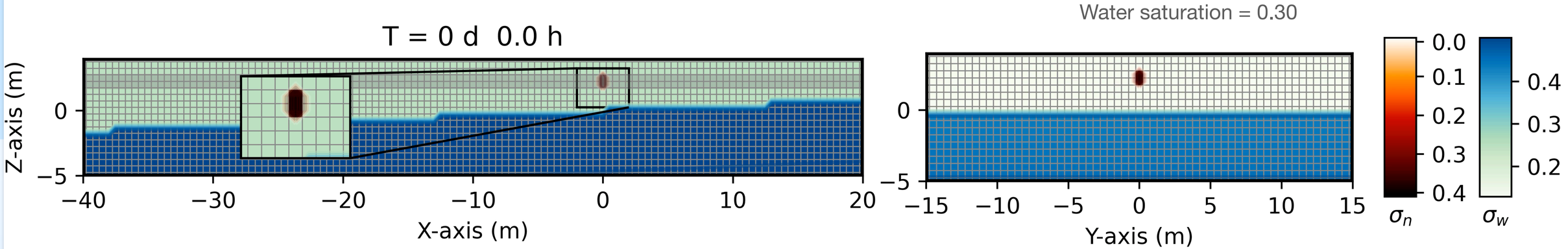
T = 0 d 0.0 h
Z-axis (m)
X-axis (m)
Water saturation = 0.30
Y-axis (m)
σ_n
σ_w

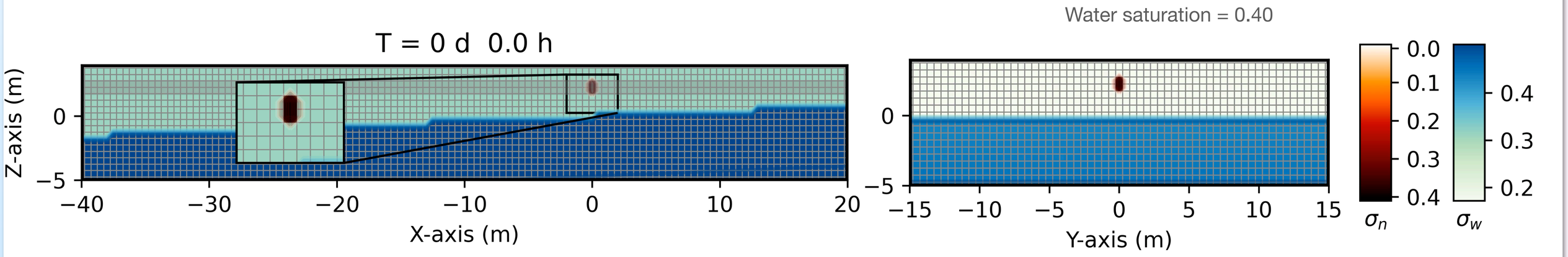
T = 0 d 0.0 h
Z-axis (m)
X-axis (m)
Water saturation = 0.40
Y-axis (m)
σ_n
σ_w

Crude Oil (Petroleum) at 5 meters from the GW

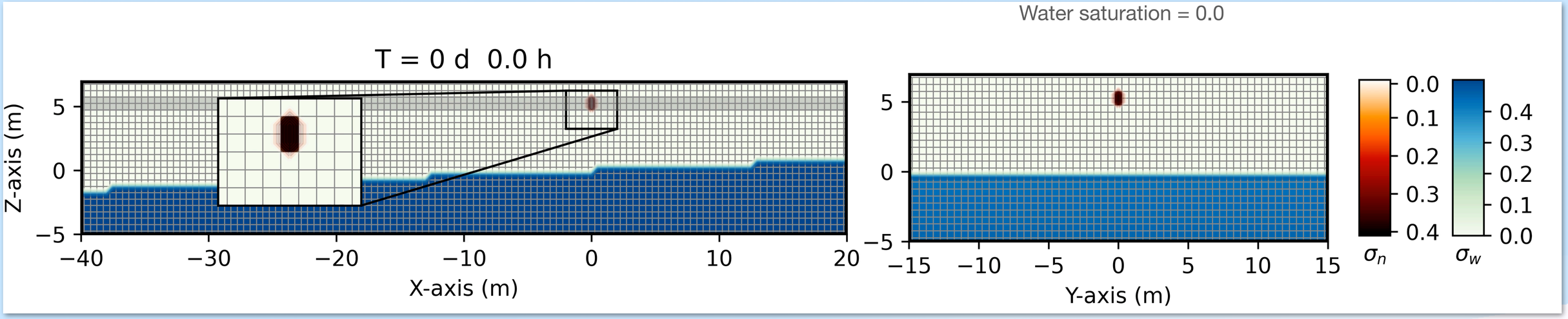

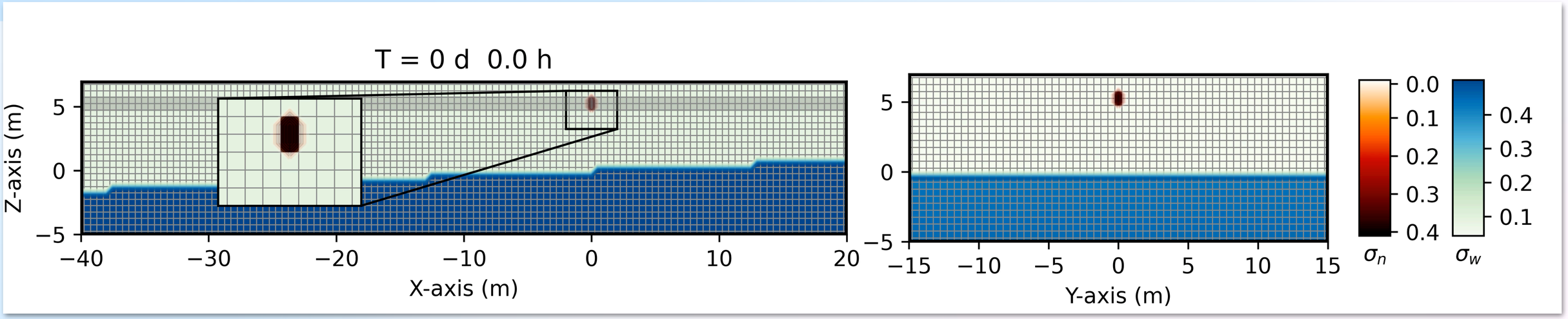

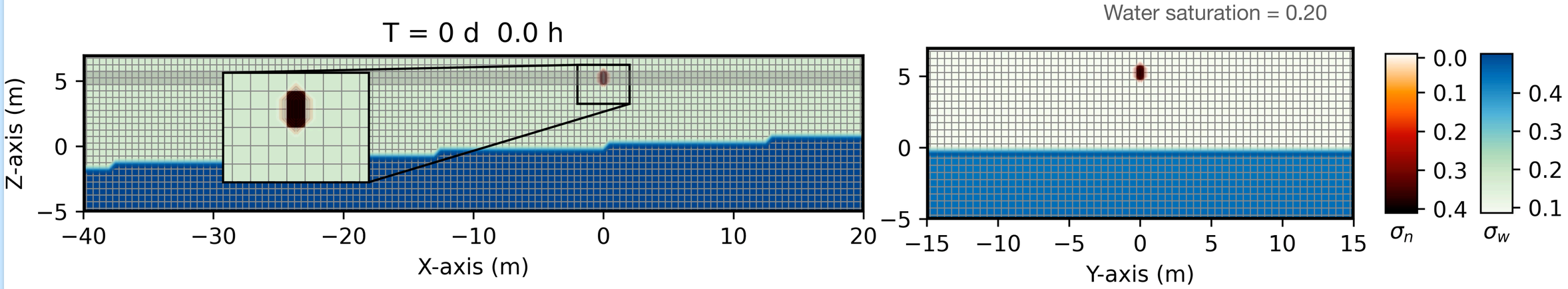
T = 0 d 0.0 h
Z-axis (m)
X-axis (m)
Water saturation = 0.20
Y-axis (m)
σ_n
σ_w

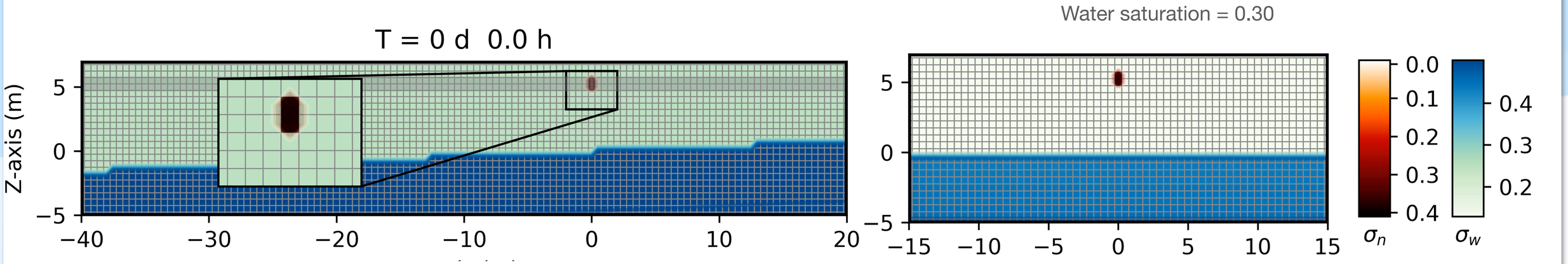
T = 0 d 0.0 h
Z-axis (m)
Water saturation = 0.30
σ_n
σ_w

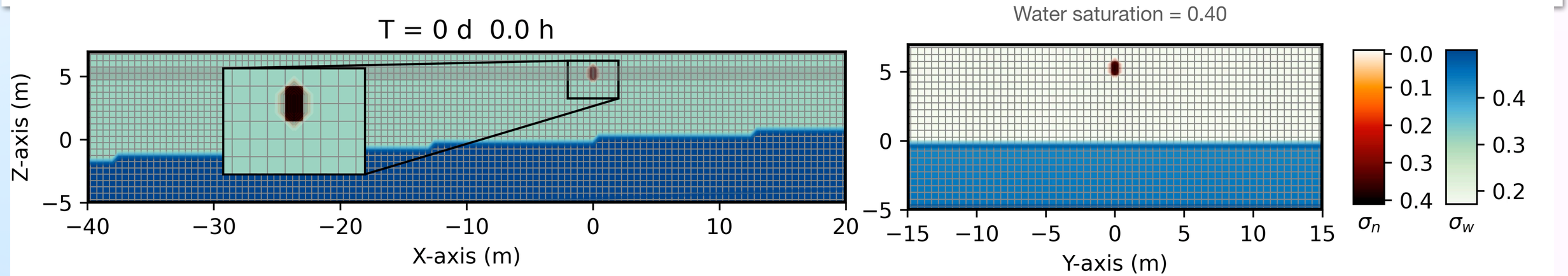
T = 0 d 0.0 h
Z-axis (m)
X-axis (m)
Water saturation = 0.40
Y-axis (m)
σ_n
σ_w

Quantitative distribution of the crude oil mass spilled

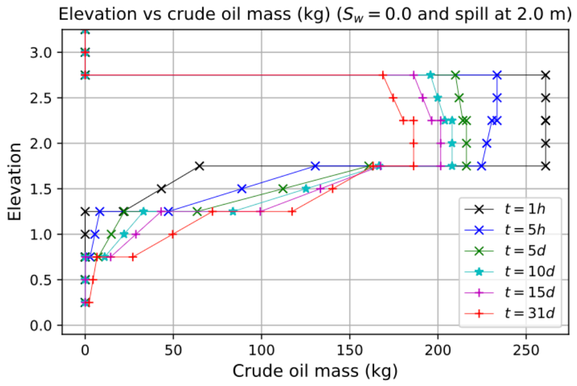

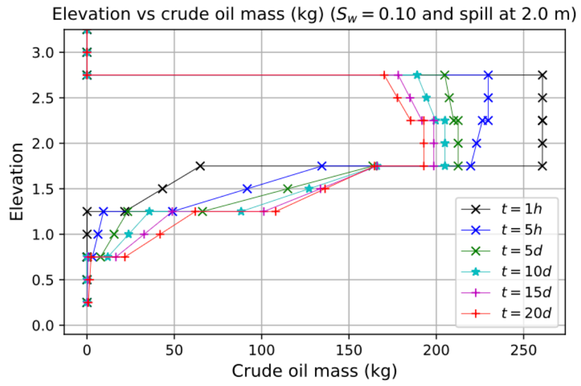

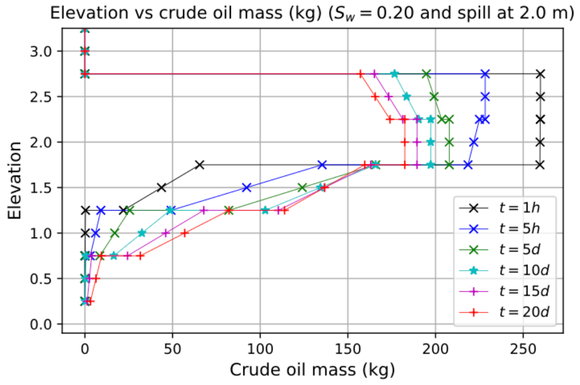

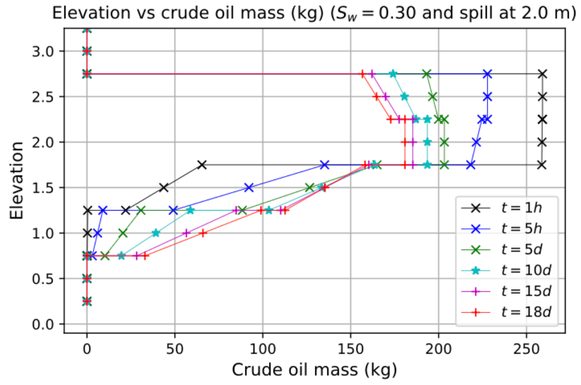

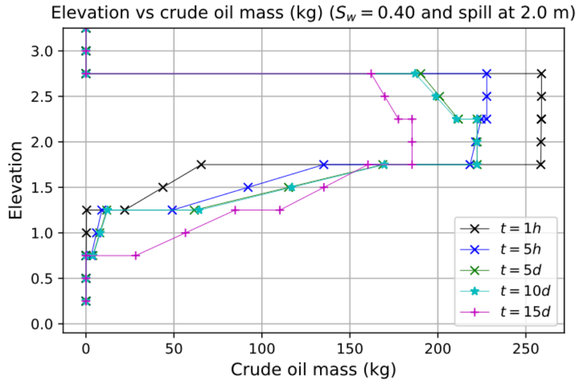

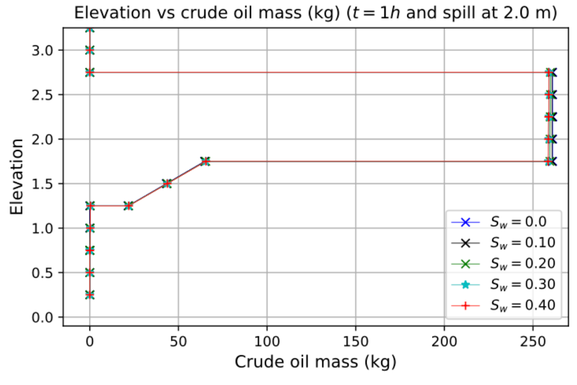

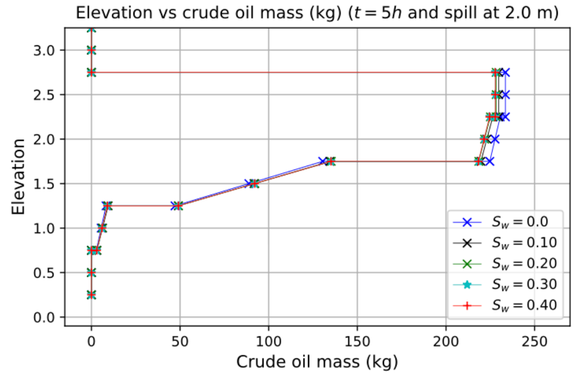

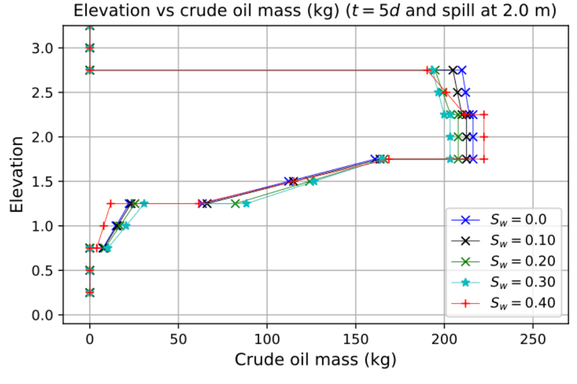

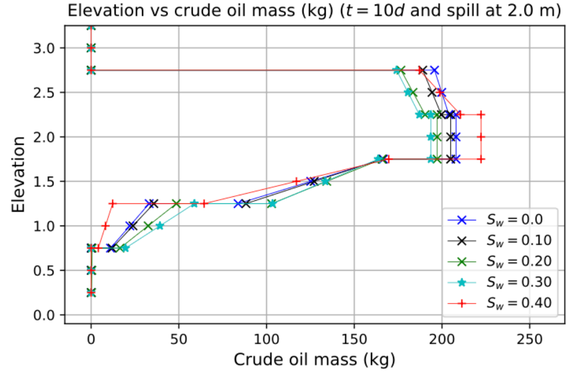

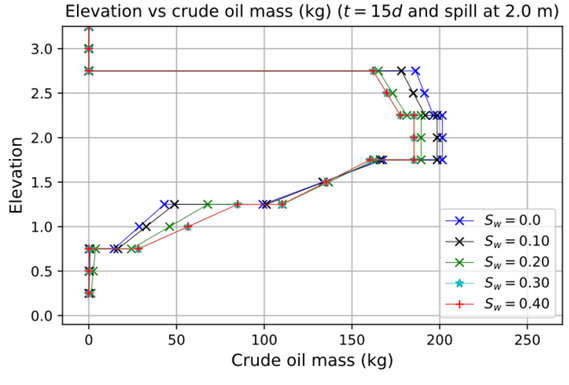

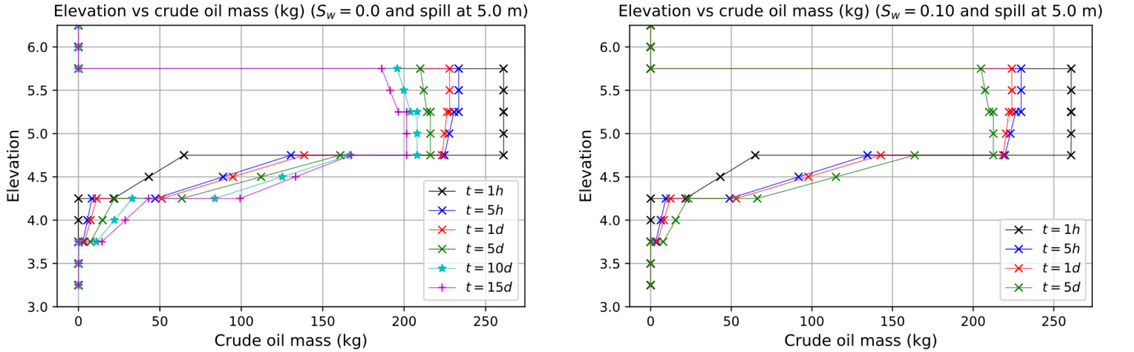
Elevation vs crude oil mass (kg) ($S_w = 0.0$ and spill at 5.0 m)
Elevation
Crude oil mass (kg)
$t = 1h$
$t = 5h$
$t = 1d$
$t = 5d$
$t = 10d$
$t = 15d$

Elevation vs crude oil mass (kg) ($S_w = 0.10$ and spill at 5.0 m)
Elevation
Crude oil mass (kg)
$t = 1h$
$t = 5h$
$t = 1d$
$t = 5d$

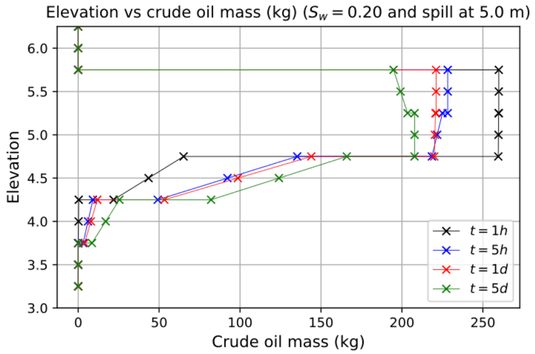
Elevation vs crude oil mass (kg) ($S_w = 0.20$ and spill at 5.0 m)
Elevation
Crude oil mass (kg)
$t = 1h$
$t = 5h$
$t = 1d$
$t = 5d$

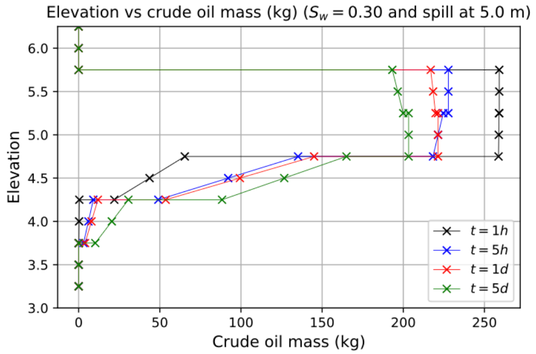
Elevation vs crude oil mass (kg) ($S_w = 0.30$ and spill at 5.0 m)
Elevation
Crude oil mass (kg)
$t = 1h$
$t = 5h$
$t = 1d$
$t = 5d$

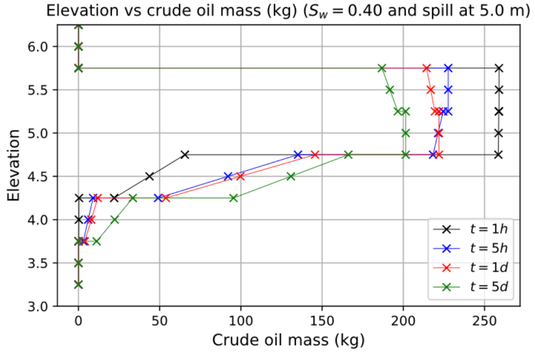
Elevation vs crude oil mass (kg) ($S_w = 0.40$ and spill at 5.0 m)
Elevation
Crude oil mass (kg)
$t = 1h$
$t = 5h$
$t = 1d$
$t = 5d$

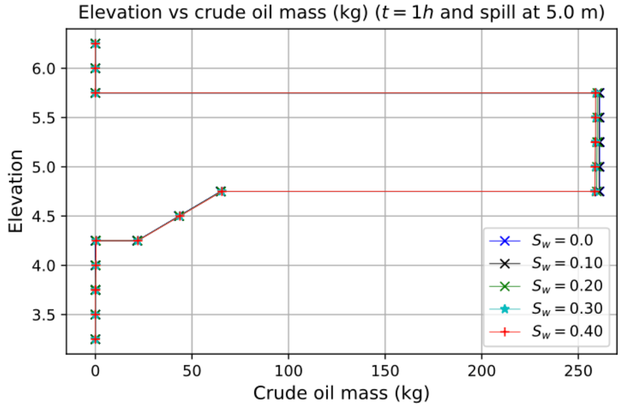
Elevation vs crude oil mass (kg) ($t = 1h$ and spill at 5.0 m)
Elevation
Crude oil mass (kg)
$S_w = 0.0$
$S_w = 0.10$
$S_w = 0.20$
$S_w = 0.30$
$S_w = 0.40$

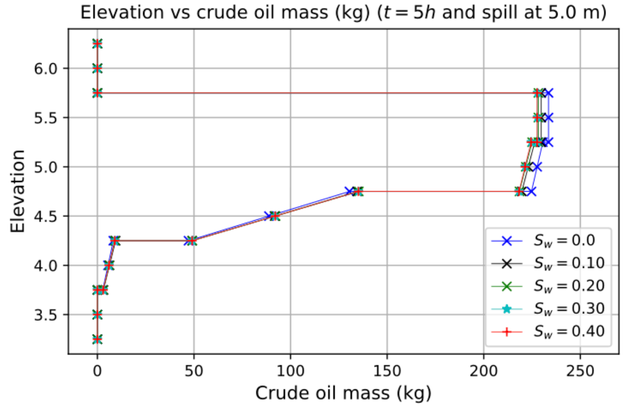
Elevation vs crude oil mass (kg) ($t = 5h$ and spill at 5.0 m)
Elevation
Crude oil mass (kg)
$S_w = 0.0$
$S_w = 0.10$
$S_w = 0.20$
$S_w = 0.30$
$S_w = 0.40$

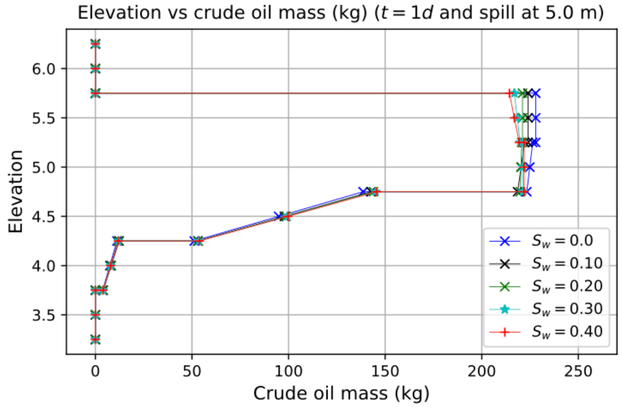
Elevation vs crude oil mass (kg) ($t = 1d$ and spill at 5.0 m)
Elevation
Crude oil mass (kg)
$S_w = 0.0$
$S_w = 0.10$
$S_w = 0.20$
$S_w = 0.30$
$S_w = 0.40$

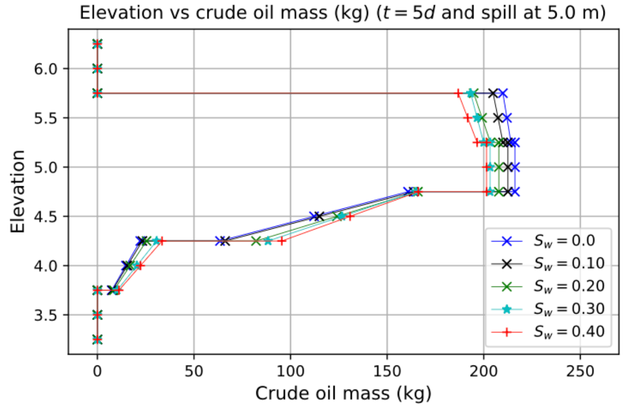
Elevation vs crude oil mass (kg) ($t = 5d$ and spill at 5.0 m)
Elevation
Crude oil mass (kg)
$S_w = 0.0$
$S_w = 0.10$
$S_w = 0.20$
$S_w = 0.30$
$S_w = 0.40$

DNAPL application: Free-Product PCE Distribution in Thick Multilayered Aquifers as Possible Long-Term Pollution Sources for Shallow and Deep Groundwaters (Parma, Northen Italy)

- A test study on Perchloroethylene (PCE) contamination in the alluvial aquifer (of Parma) was carried out. This aquifer consisting of alternating layers of low-permeability (silt and clay) and high-permeability (gravel and sand) materials. Various undulations characterize the contact surface between the aquifer and the basal aquiclude. The surface waters are shallow and are recharged by local infiltrations and by the Taro river, which is hydraulically connected to the aquifer.
- PCE contamination was monitored (from 2002 to 2019) through institutional piezometers of the municipality of Parma located throughout the urban area of Parma and showed a cyclical variation with the highest values at the beginning of recharge and the lowest when there is a recession. The persistence of PCE in the aquifer, its cyclical variation, and the almost constant peak concentration value indicates the presence of a pool.
- From the reconstruction of the 3D stratigraphic profiles, we have identified the area from which any releases of DNAPL could cause widespread and deep contamination of the aquifers downstream.

Parameter	Symbol	Value
Absolute permeability (gravel and sand)	k_{gs}	5.102×10^{-12} m^2
Absolute permeability (silt and clay)	k_{sc}	5.102×10^{-14} m^2
Rock compressibility	c_R	4.35×10^{-7} Pa^{-1}
Porosity	ϕ_0	0.37
Water viscosity	μ_w	10^{-3} kg/(ms)
Water density	ρ_w	10^3 kg/m^3
DNAPL viscosity	μ_n	0.844×10^{-3} kg/(ms)
DNAPL density	ρ_n	1643 kg/m^3
Air viscosity	μ_a	1.8×10^{-5} kg/(ms)
Air density	ρ_a	1.225 kg/m^3
Van Genuchten	(n, m)	$\left(2.68, 1 - \frac{1}{2.68}\right)$
Irreducible wetting phase saturation	S_{wir}	0.045
Surface tension air–water	σ_{aw}	7.199×10^{-2} N/m
Interfacial tension non-aqueous–water	σ_{nw}	4.44×10^{-2} N/m
Capillary pressure air–water at zero saturation	p_{caw0}	676.55 Pa
Capillary pressure air–non-aqueous at zero saturation	p_{can0}	259.83 Pa

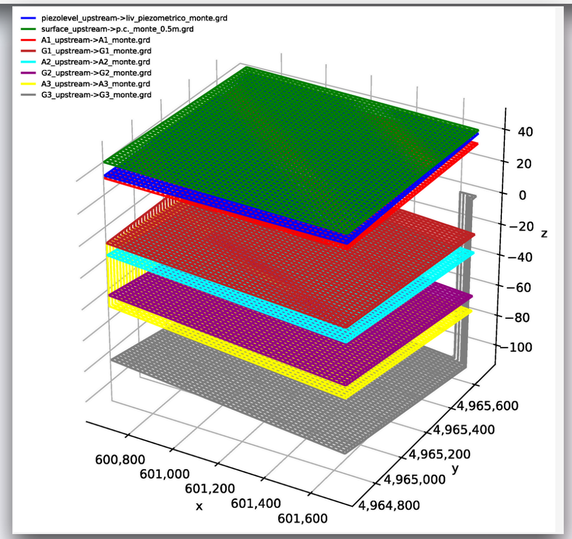

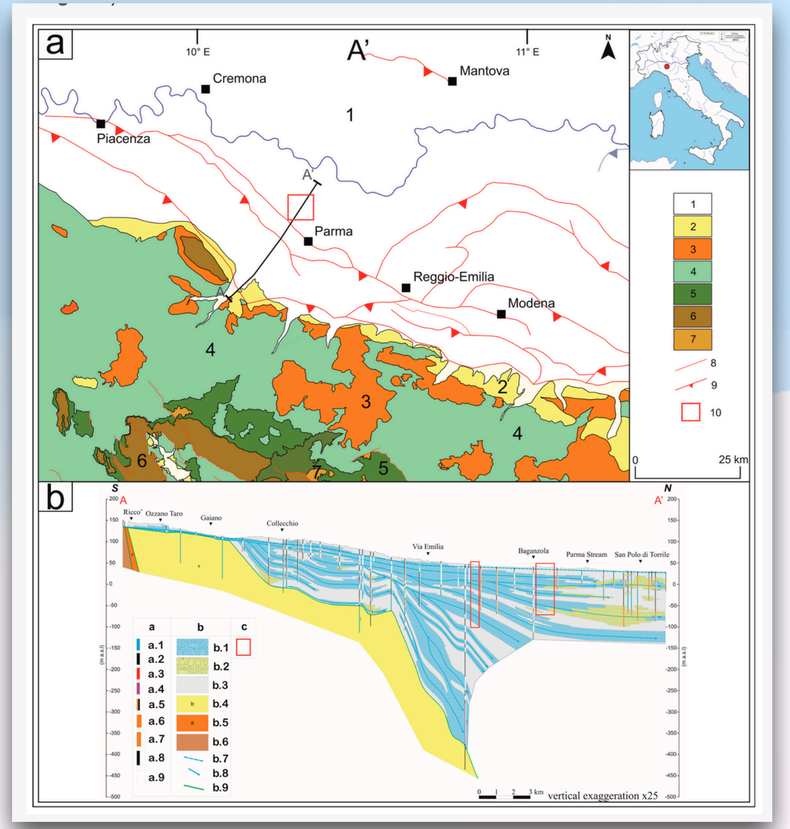

- The upstream scenario (monte)

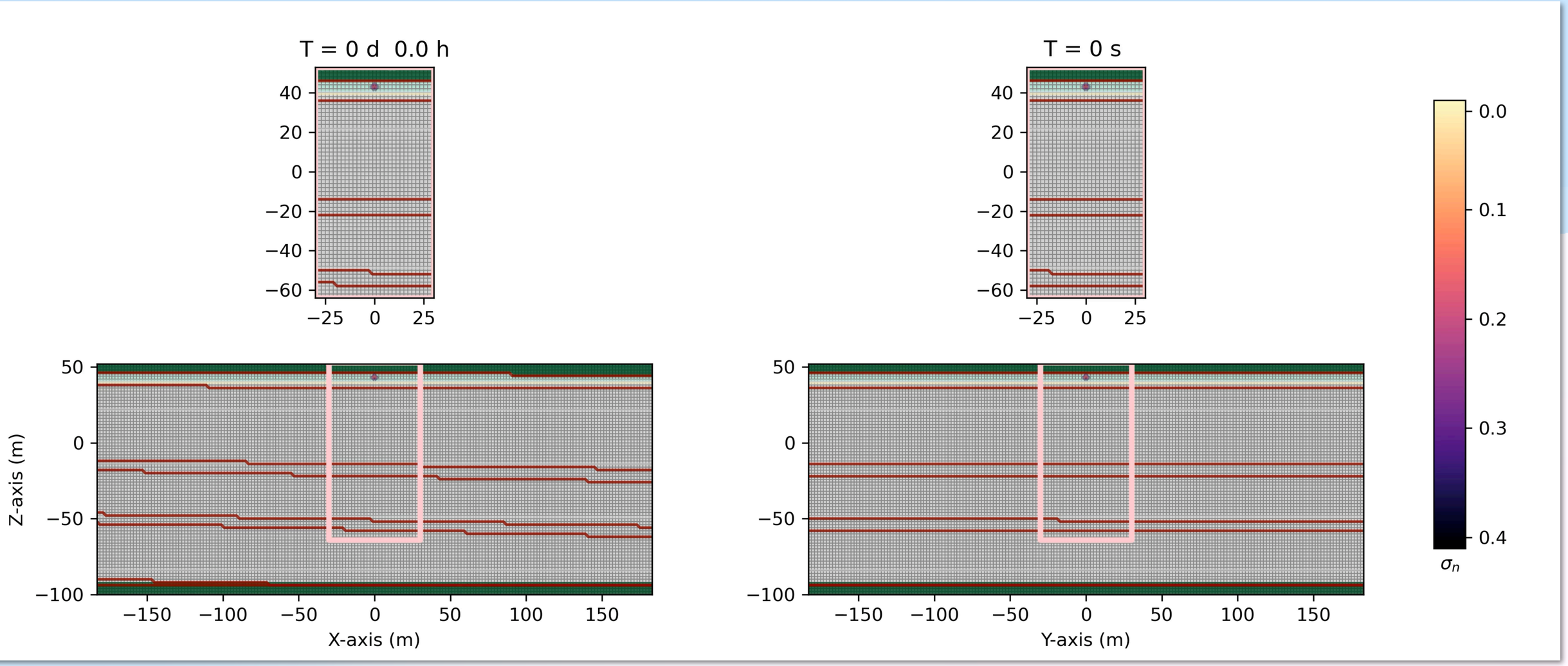

- The downstream scenario (valle)

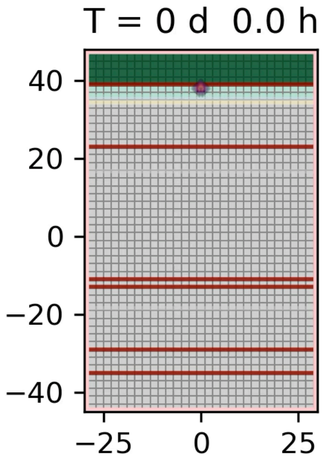

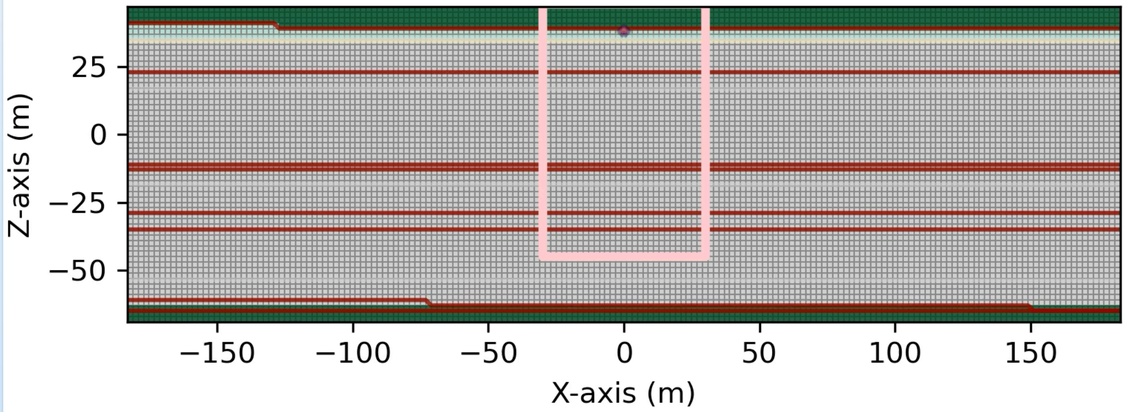

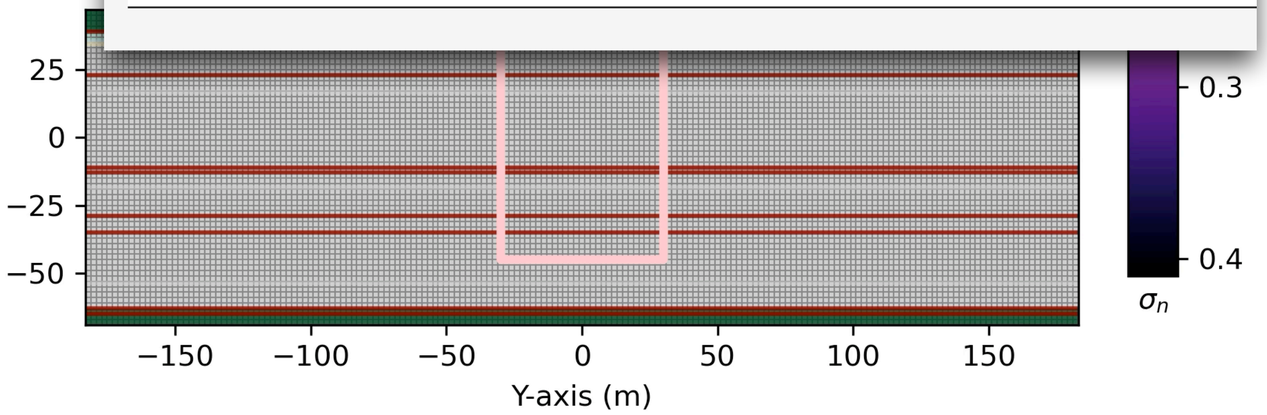

Table 5. Mass in Kg of the contaminant after 2585 days in the downstream aquifer scenario and the percentual of contaminant in the different levels in terms of z-coordinate. Notice that the sum is 100%.

Downstream Aquifer Scenario			
z Altitude (m a.s.l.)	**Type of Layer**	**Mass in kg of PCE After 2585 Days**	**Percentage of Contaminant Trapped (%)**
39 < z < 47	-	0.0	0.00
23 < z < 39	Silt and clay	2093.8	43.06
−9 < z < 23	Gravel and sand	739.3	15.20
−13 < z < −9	Silt and clay	534.2	10.98
−27 < z < −13	Gravel and sand	771.4	15.86
−31 < z < −27	Silt and clay	625.4	12.86
−49 < z < −31	Gravel and sand	99.2	2.04
−71 < z < −49	-	0.0	0.00

Numerical Simulations of Free-Product DNAPL Extraction in Potential Emergency Scenarios: A Test Study in a PCE-Contaminated Alluvial Aquifer (Parma, Northern Italy)

Figure 4. (**a**) Aquiclude base contour map and location of the modeled area. (**b**) Detailed stratigraphic sections (a, b, c, d).

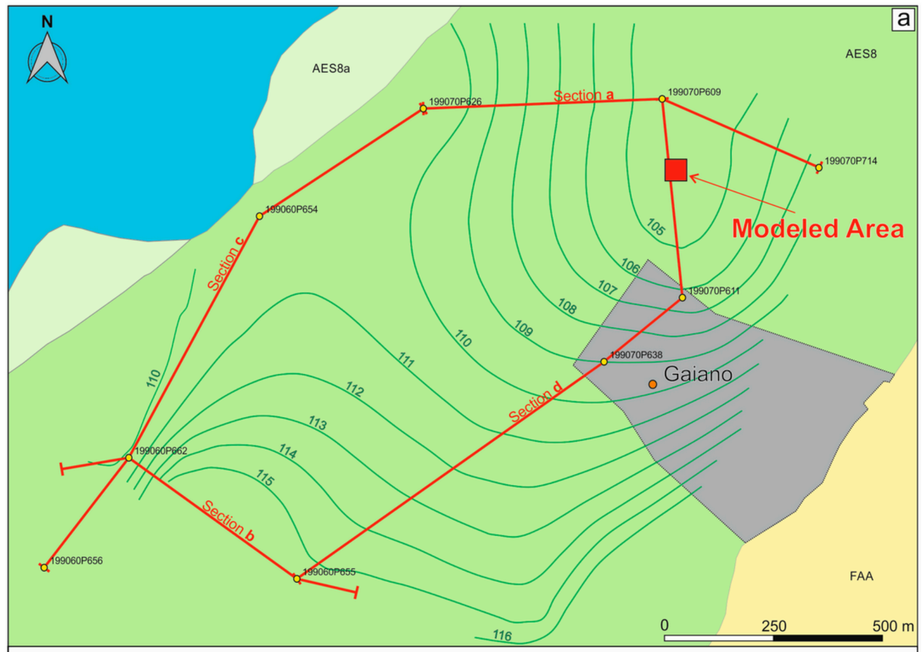

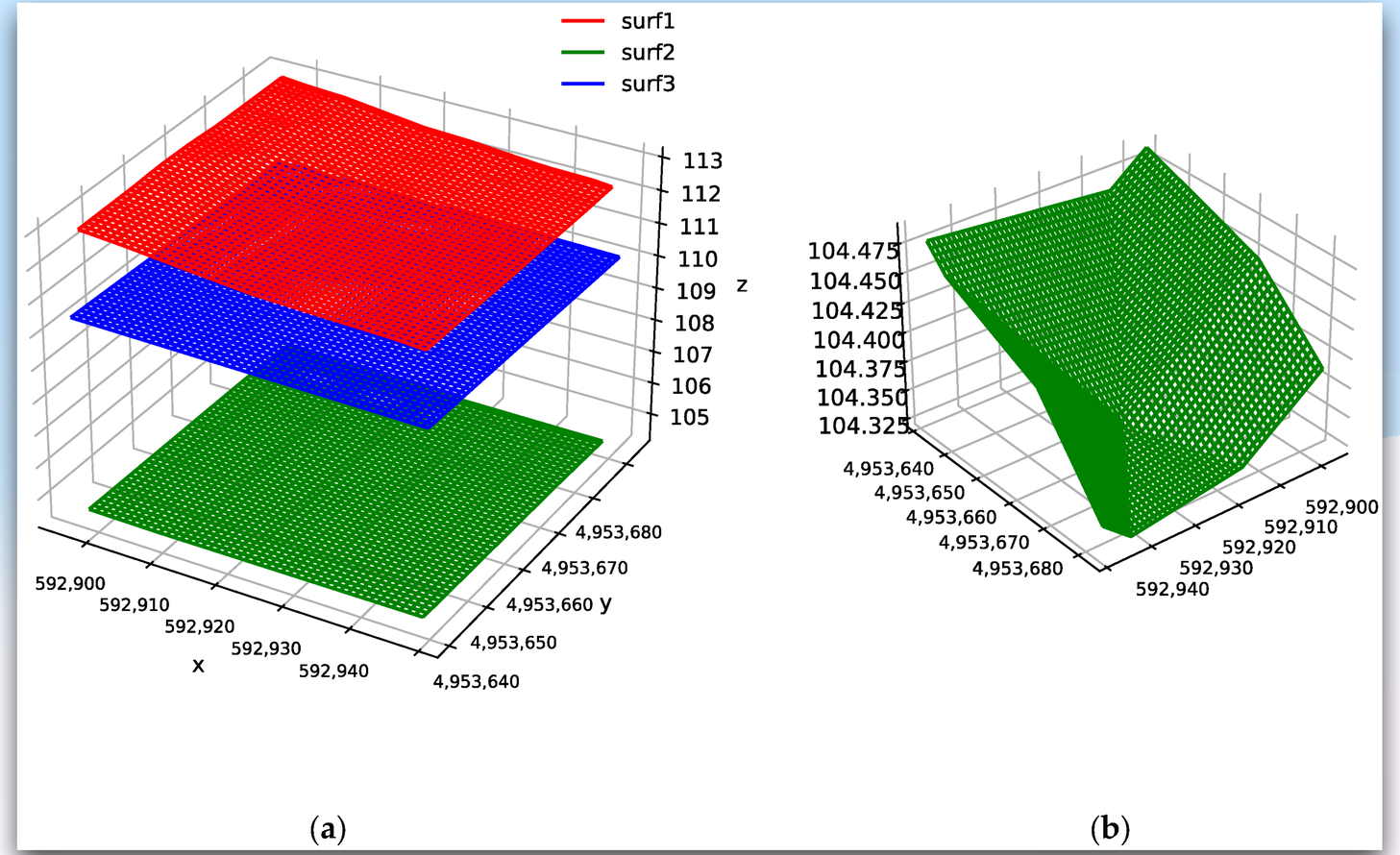

Figure 5. The three surfaces with georeferenced coordinates: (**a**) the three surfaces, i.e., the aquifer bottom surface (surf2-green), the upper-level topographic surface (surf1-red), and the groundwater table surface (surf3-blue); (**b**) a zoom of the aquifer bottom surface that highlights a depression in the base aquiclude (see Figure 4).

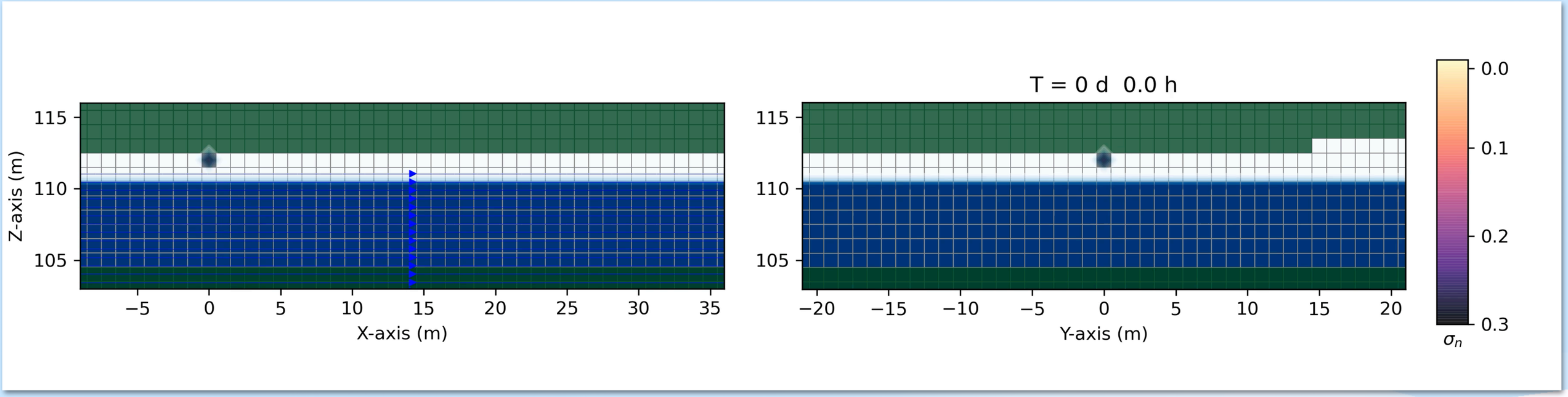
T = 0 d 0.0 h
Z-axis (m)
X-axis (m)
Y-axis (m)
115
110
105
−5 0 5 10 15 20 25 30 35
−20 −15 −10 −5 0 5 10 15 20
0.0
0.1
0.2
0.3
σ_n

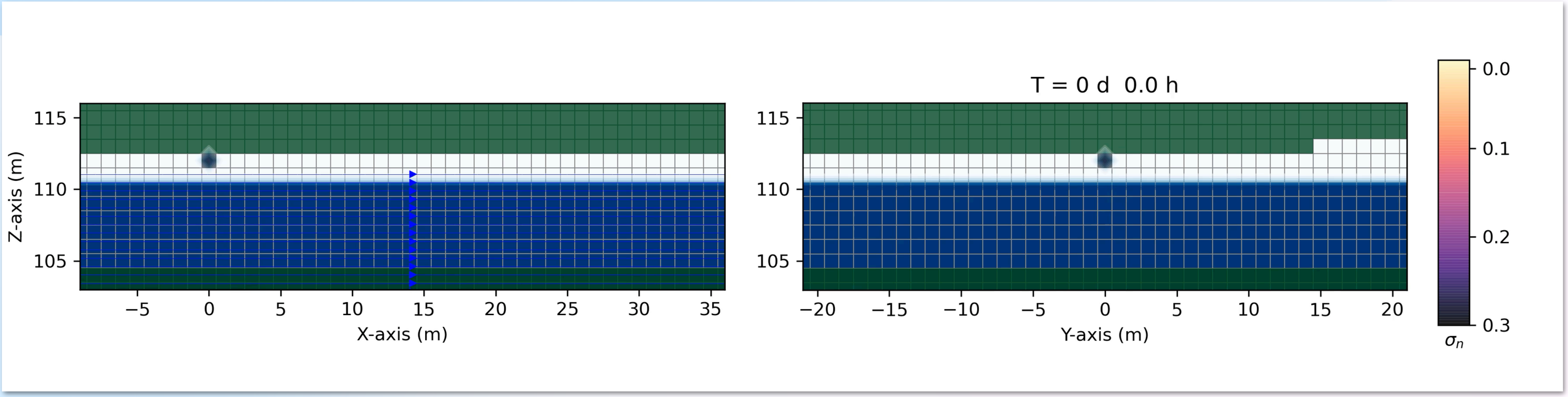
T = 0 d 0.0 h
Z-axis (m)
X-axis (m)
Y-axis (m)
115
110
105
−5 0 5 10 15 20 25 30 35
−20 −15 −10 −5 0 5 10 15 20
0.0
0.1
0.2
0.3
σ_n

Migration of DNAPL in a saturated porous media: validation of HRSC numerical simulations through a sandbox experiment

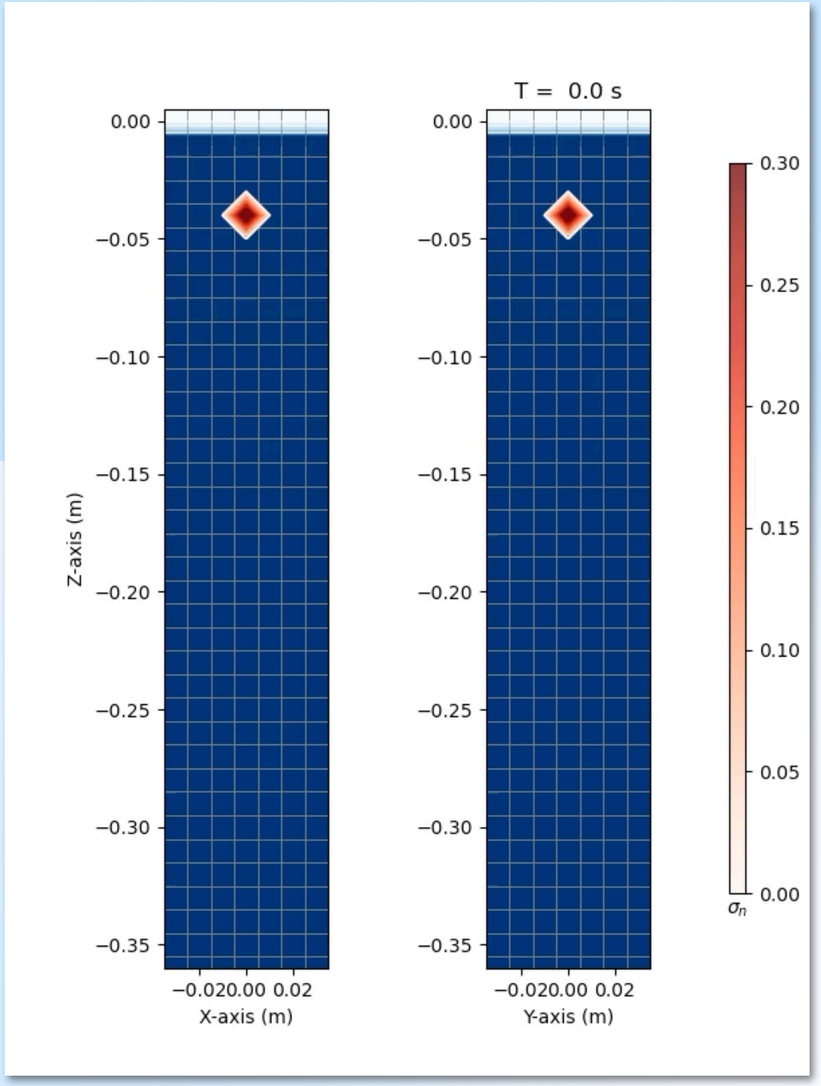

Figure 1. Experimental equipment for the column filled with glass beads of 1 mm diameter as the porous media and saturated with water and fluorescein.

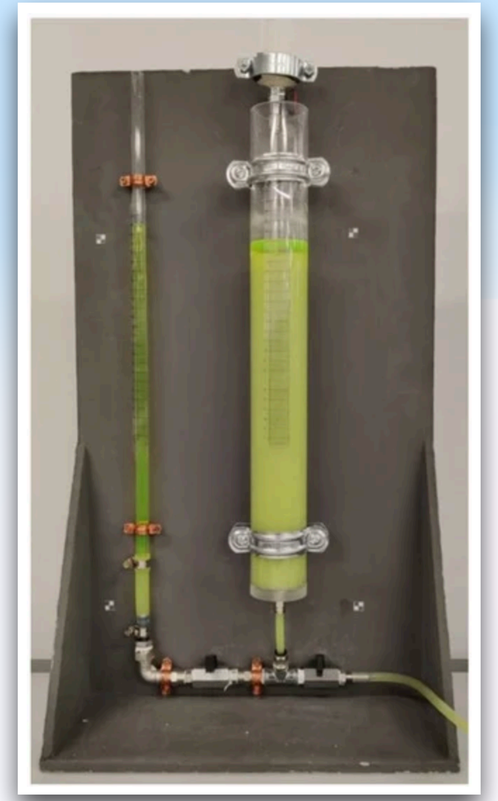

hydrofluoroether (HFE-7100)

Table 1. List of parameters used for the three-dimensional numerical simulations of a DNAPL leak in a column.

Parameter	Symbol	Value
Absolute permeability, m^2	k	6.122×10^{-10}
Rock compressibility, Pa^{-1}	c_R	4.35×10^{-7}
Porosity	ϕ_0	0.37
Water viscosity, $\mathrm{kg}/(\mathrm{ms})$	μ_w	10^{-3}
Water density, kg/m^3	ρ_w	10^3
DNAPL HFE-7100 dynamic viscosity, $\mathrm{kg}/(\mathrm{ms})$	μ_n	1.35×10^{-3}
DNAPL HFE-7100 density, kg/m^3	ρ_n	1500
Air viscosity, $\mathrm{kg}/(\mathrm{ms})$	μ_a	1.8×10^{-5}
Air density, kg/m^3	ρ_a	1.225
Van Genuchten parameter	(n, m)	(2.68,0.627)
Irreducible wetting phase saturation	S_{wir}	0.045
Surface tension DNAPL, N/m	σ_{na}	13.60×10^{-3}
Interfacial tension DNAPL, N/m	σ_{nw}	35.59×10^{-3}
Surface tension water, N/m	σ_{aw}	71.75×10^{-3}
Capillary pressure air-water at zero saturation, Pa	p_{caw0}	676.55
Capillary pressure DNAPL-water at zero saturation, Pa	p_{cnw0}	334.93
Capillary pressure air-nonaqueous at zero saturation, Pa	p_{can0}	341.62
Resolution, m	$\Delta x = \Delta y = \Delta z$	0.01

Figure 5. Comparison between the experimental results on the DNAPL migration in a column and three-dimensional numerical results on the saturation contours ($\sigma_n = S_n\phi$) of the DNAPL in a column using a grid dimension of $0.060\ \mathrm{m} \times 0.060 \times 0.360\ \mathrm{m}$, at different times: 12 s, 24 s, 50 s, 90 s. The left-hand side of each panel time shows the experimental result, while the saturation contours of the DNAPL migration in the $(z - x)$ plane are placed on the right-hand side of each panel.

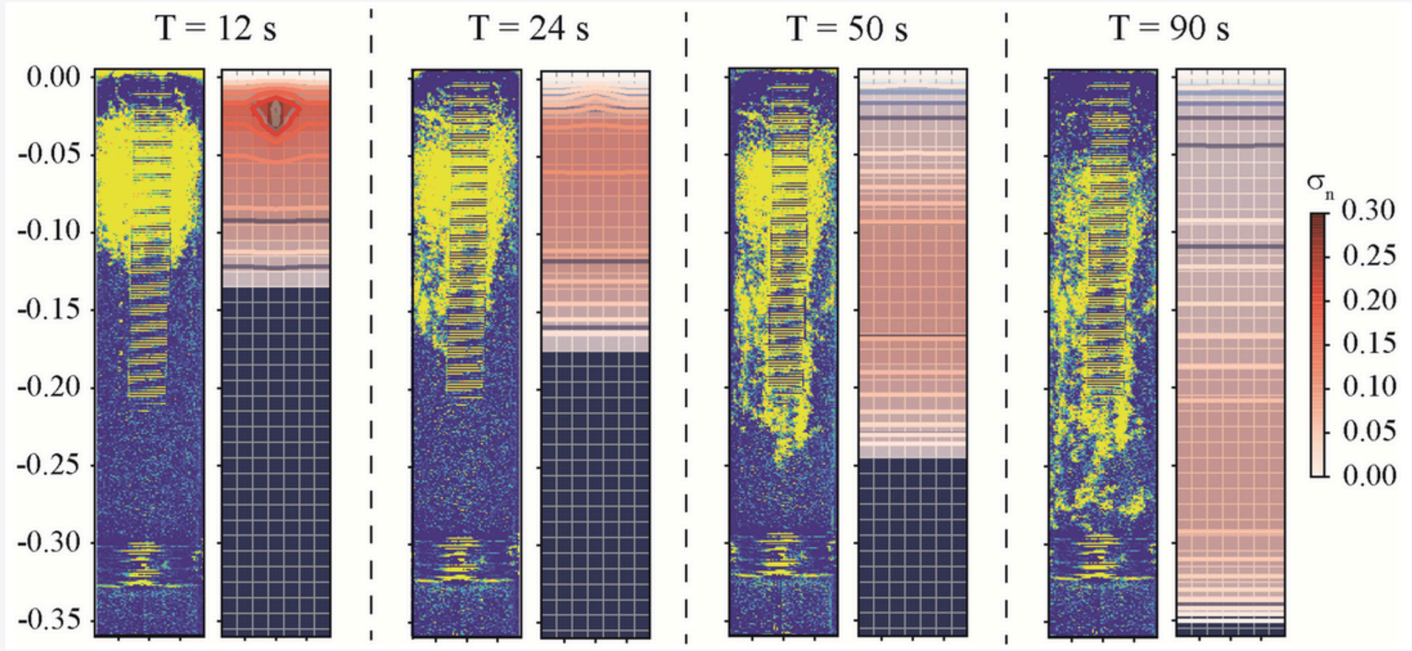

3 seconds

Table 2. Values of the position of the contaminant migration in the column experiment, and in the numerical model output, for different times.

Time (s)	Position of the Contaminant in the Experimental Column (m)	Position of the Contaminant in the Numerical Model (m)
12	−0.125	−0.135
24	−0.170	−0.175
50	−0.240	−0.245
90	−0.320	−0.350

Figure 6. Comparison between the experimental results on the DNAPL migration in a sandbox and three-dimensional numerical results on the saturation contours ($\sigma_n = S_n\phi$) of the DNAPL in a sandbox using a grid dimension of $0.060\ \mathrm{m} \times 0.060 \times 0.360\ \mathrm{m}$ at different times: 5 s, 25 s, 50 s, 75 s, respectively. The left-hand side of each panel time shows the experimental result in the sandbox, while the saturation contours of the DNAPL migration in the $(z - x)$ plane are placed on the right-hand side of each panel.

Figure 2. Sketch of the experimental device. Constant head boundaries upstream and downstream; the porous media was laterally confined by iron plates, and at the top, it is involved in the capillary fringe. The red dot is the source location. Dimensions are in mm. The blue arrow indicates the flow direction.

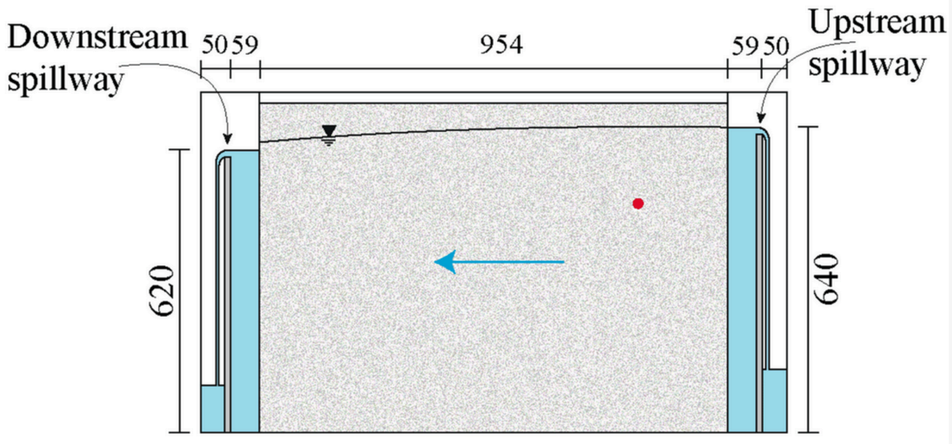

Table 3. Values of the position of the contaminant migration in the sandbox experiment, and in the numerical model output, for different times.

Time (s)	Position of the Contaminant in the Experimental Sandbox (m)	Position of the Contaminant in the Numerical Model (m)
5	−0.200	−0.225
25	−0.280	−0.335
50	−0.380	−0.435
75	−0.435	−0.480

45 seconds

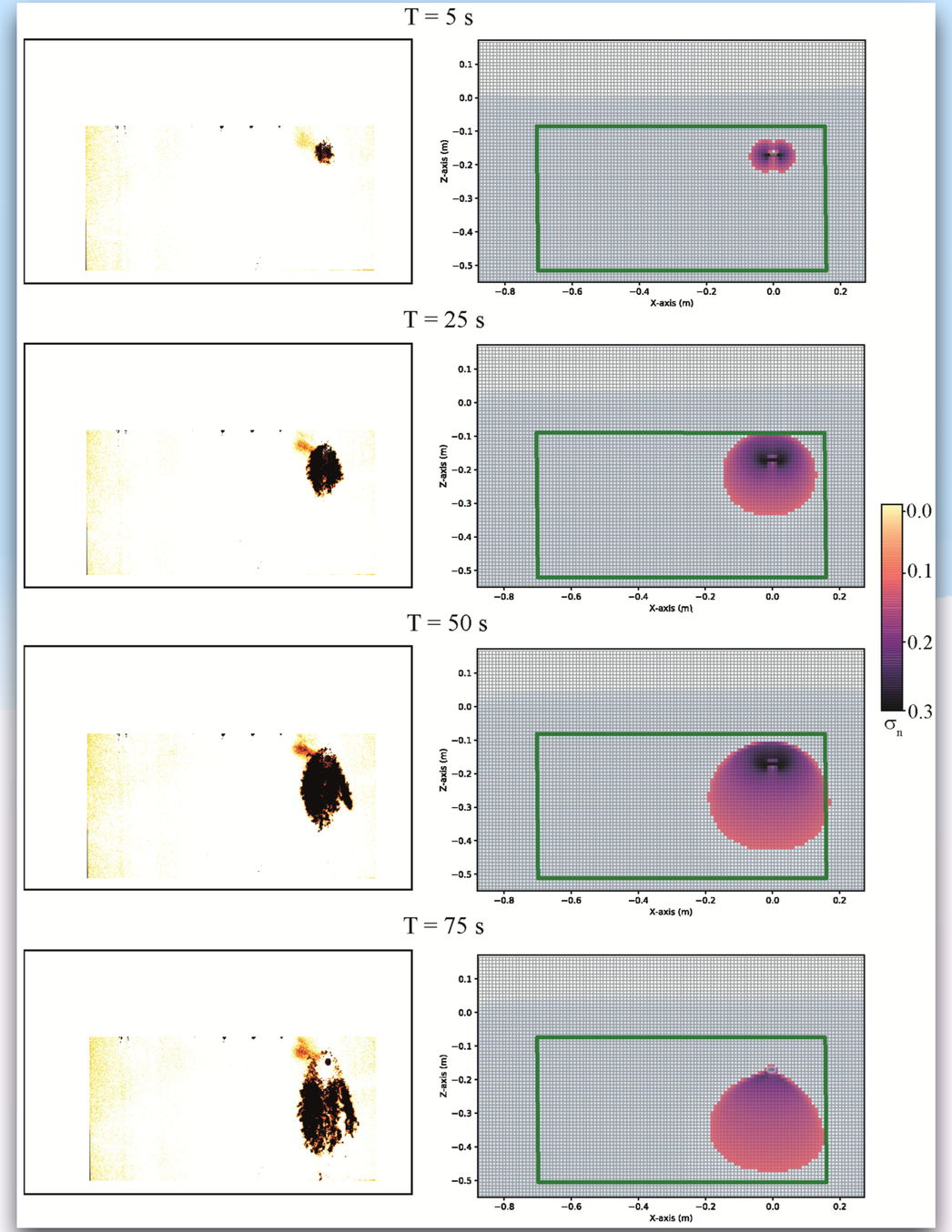

Feo, Celico, Zanini, Water 2023

Recent Publications

- **Feo, A**; Pasquali, M; Celico, F. Building a Sustainable Transportation Path for Crude Oil to Minimize Emergency Scenarios. **2026**
- **Feo, A**.; Celico, F. Influence of Spill Pressure and Saturation on the Migration and Distribution of Diesel Oil Contaminant in Unconfined Aquifers Using Three-Dimensional Numerical Simulations. Appl. Sci. **2025,** 15, 9303. https://doi.org/10.3390/app15179303
- **Feo, A**.; Pinardi, R.; Artoni, A.; Celico, F. Estimation of Free-Product PCE Distribution in Thick Multilayered Aquifers as Possible Long-Term Pollution Sources for Shallow and Deep Groundwaters, Using High-Precision Numerical Simulations. Water **2024**, 16, 3053. https://doi.org/10.3390/w16213053
- **Feo, A**.; Celico, F.; Zanini, A. Migration of DNAPL in Saturated Porous Media: Validation of High-Resolution Shock-Capturing Numerical Simulations through a Sandbox Experiment. Water **2023**, 15, 1471. https://doi.org/10.3390/w15081471
- **Feo, A**.; Pinardi, R.; Scanferla, E.; Celico, F. How to Minimize the Environmental Contamination Caused by Hydrocarbon Releases by Onshore Pipelines: The Key Role of a Three-Dimensional Three-Phase Fluid Flow Numerical Model. Water **2023**, 15, 1900. https://doi.org/10.3390/w15101900
- **Feo, A**.; Pinardi, R.; Artoni, A.; Celico, F. Three-Dimensional High-Precision Numerical Simulations of Free-Product DNAPL Extraction in Potential Emergency Scenarios: A Test Study in a PCE-Contaminated Alluvial Aquifer (Parma, Northern Italy). Sustainability **2023**, 15, 9166. https://doi.org/10.3390/su15129166
- **Feo, A**.; Lo Medico, F.; Rizzo, P.; Morticelli, M.G.; Pinardi, R.; Rotigliano, E.; Celico, F. How to Predict the Efficacy of Free-Product DNAPL Pool Extraction Using 3D High-Precision Numerical Simulations: An Interdisciplinary Test Study in South-Western Sicily (Italy). Hydrology **2023**, 10, 143. https://doi.org/10.3390/hydrology10070143
- **Feo, A**.; Celico, F. Investigating the migration of immiscible contaminant fluid flow in homogeneous and heterogeneous aquifers with high-precision numerical simulations. PLoS ONE **2022**, 17, e0266486.
- **Feo, A**.; Celico, F. High-resolution shock-capturing numerical simulations of three-phase immiscible fluids from the unsaturated to the saturated zone. Sci. Rep. **2021**, 11, 5212.

Thank you!